Supplemental material to this article can be found at:
http://molpharm.aspetjournals.org/content/suppl/2022/11/16/molpharm.122.000614.DC1

1521-0111/103/1/21–37$35.00
MOLECULAR PHARMACOLOGY

dx.doi.org/10.1124/molpharm.122.000614
Mol Pharmacol 103:21–37, January 2023

Functional Assessment of Cancer-Linked Mutations in Sensitive Regions of Regulators of G Protein Signaling Predicted by Three-Dimensional Missense Tolerance Ratio Analysis[S]

Carolina Montañez-Miranda, Riley E. Perszyk, Nicholas H. Harbin, Jennifer Okalova, Suneela Ramineni, Stephen F. Traynelis, and John R. Hepler

Department of Pharmacology and Chemical Biology (C.M.-M., R.E.P., N.H.H., S.R., S.F.T., J.R.H.) and Aflac Cancer and Blood Disorders Center, Department of Pediatrics (J.O.), Emory University School of Medicine, Atlanta, Georgia

Received August 16, 2022; accepted October 18, 2022

ABSTRACT

Regulators of G protein signaling (RGS) proteins modulate G protein–coupled receptor (GPCR) signaling by acting as negative regulators of G proteins. Genetic variants in RGS proteins are associated with many diseases, including cancers, although the impact of these mutations on protein function is uncertain. Here we analyze the RGS domains of 15 RGS protein family members using a novel bioinformatic tool that measures the missense tolerance ratio (MTR) using a three-dimensional (3D) structure (3DMTR). Subsequent permutation analysis can define the protein regions that are most significantly intolerant ($P < 0.05$) in each dataset. We further focused on RGS14, RGS10, and RGS4. RGS14 exhibited seven significantly tolerant and seven significantly intolerant residues, RGS10 had six intolerant residues, and RGS4 had eight tolerant and six intolerant residues. Intolerant and tolerant-control residues that overlap with pathogenic cancer mutations reported in the COSMIC cancer database were selected to define the functional phenotype. Using complimentary cellular and biochemical approaches, proteins were tested for effects on GPCR-Gα activation, Gα binding properties, and downstream cAMP levels. Identified intolerant residues with reported cancer-linked mutations RGS14-R173C/H and RGS4-K125Q/E126K, and tolerant RGS14-S127P and RGS10-S64T resulted in a loss-of-function phenotype in GPCR-G protein signaling activity. In downstream cAMP measurement, tolerant RGS14-D137Y and RGS10-S64T and intolerant RGS10-K89M resulted in change of function phenotypes. These findings show that 3DMTR identified intolerant residues that overlap with cancer-linked mutations cause phenotypic changes that negatively impact GPCR-G protein signaling and suggests that 3DMTR is a potentially useful bioinformatics tool for predicting functionally important protein residues.

SIGNIFICANCE STATEMENT

Human genetic variant/mutation information has expanded rapidly in recent years, including cancer-linked mutations in regulator of G protein signaling (RGS) proteins. However, experimental testing of the impact of this vast catalogue of mutations on protein function is not feasible. We used the novel bioinformatics tool three-dimensional missense tolerance ratio (3DMTR) to define regions of genetic intolerance in RGS proteins and prioritize which cancer-linked mutants to test. We found that 3DMTR more accurately classifies loss-of-function mutations in RGS proteins than other databases thereby offering a valuable new research tool.

Introduction

Since the publication of the human genome and the development of bioinformatic sequencing tools, human genetic variant information is being identified rapidly. These advances led to the creation of many publicly available databases that reflect both healthy and diseased human populations. However, experimental testing of the vast catalog of identified mutations is simply not feasible. Missense mutations are genetic variations where a single base pair substitution produces a different amino acid at the same position. Variations in protein structure can affect folding, stability and aggregation, thereby affecting the function of signaling proteins (Thusberg and Vihinen, 2009). Functionally relevant genetic variation has been reported in many proteins, including the regulators of G protein signaling (RGS) (Squires et al., 2021).

RGS proteins play a vital role modulating G protein–coupled receptor (GPCR)-G protein signaling events. All RGS proteins share an evolutionary conserved RGS domain that binds active Gα subunits and acts as GTPase accelerating

Funding for this work was provided by National Institutes of Health National Institute of Neurological Disorders and Stroke [Grant NS037112] (to J.R.H.) and [Grant NS111619] (to S.F.T.) and National Institute of General Medical Science [Grant GM140632] (to J.R.H.).
No author has an actual or perceived conflict of interest with the contents of this article.
Primary laboratory of origin: Hepler Laboratory (Department of Pharmacology and Chemical Biology, Emory University School of Medicine, Atlanta, GA).
dx.doi.org/10.1124/molpharm.122.000614.
[S] This article has supplemental material available at molpharm.aspetjournals.org.

ABBREVIATIONS: α2AR, alpha 2 adrenergic receptor; AC, adenylyl cyclase; BRET, bioluminescence resonance energy transfer; CoF, change of function; 3D, three-dimensional; DMEM, Dulbecco's modified Eagle's medium; FSK, forskolin; GAP, GTPase accelerating protein; GEF, guanine nucleotide exchange factor; gnomAD, Genome Aggregation Database; GPCR, G protein–coupled receptor; HEK, human embryonic kidney; LoF, loss of function; MTR, missense tolerance ratio; RGS, regulator of G protein signaling; WT, wild-type.

proteins (GAPs), negatively regulating GPCR-Gα signaling (Tesmer et al., 1997; Hollinger and Hepler, 2002; Willars, 2006). Outside of their GAP function, RGS proteins competitively bind active Gα and receptors to promote the rapid cycling of Gα subunits between active and inactive states (McCoy and Hepler, 2009).

Recent deep sequencing studies have shown GPCR-G protein complexes to be frequently mutated in cancer (Kan et al., 2010; O'Hayre et al., 2013; DiGiacomo et al., 2020). GPCRs are expressed in cancerous tissues and mediate proliferation, survival, invasion, and metastasis (Gutkind 1998; Hurst and Hooks, 2009). The pro-oncogenic effects of overexpressed constitutively activating mutations in GPCRs (O'Hayre et al., 2013; Moore et al., 2016; Wright et al., 2019; DiGiacomo et al., 2020) and Gα subunit (Van Raamsdonk et al., 2009, 2010; Wu et al., 2011; Nairismagi et al., 2016; Ideno et al., 2018 ;DiGiacomo et al., 2020) have led to enhanced downstream signaling in reported cancer studies. Cancer-derived activated mutations in Gαo can induce oncogenic transformation (Garcia-Marcos et al., 2011), while inactivated mutations in Gαi/o-receptors can lead to enhanced cAMP activity (Chaudhary and Kim, 2021). These studies suggest that the loss of Gαbinding and GAP function in RGS proteins can promote oncogenic activity.

Multiple sequence-based analytical tools provide information and predictions about evolutionary conserved areas of a protein that are vital for structure and function (Nobrega and Pennacchio, 2004). Interestingly, sequence-based tools, like missense tolerance ratio (1DMTR) (Traynelis et al., 2017) and SIFT, access the same genetic variant databases to run their algorithms but interpret the predictive effect of a mutation in different ways. Recently, a novel tool known as three-dimensional missense tolerance ratio (3DMTR) permutation analysis (Perszyk et al., 2021) has been developed but not yet widely tested. The improved 3DMTR algorithm calculates the missense tolerance ratio for the neighboring residues in three-dimensional (3D) distance from protein crystallography or cryo-EM data.

RGS proteins are divided in subfamilies based on sequence homology and other shared domains (Hepler, 1999; Willars, 2006; Sjogren and Neubig, 2010; Stewart and Fisher, 2015). Here we analyzed the RGS domains of 15 RGS proteins with reported structures and focused on assessing three RGS proteins in particular: RGS14, RGS10, and RGS4. RGS14 and RGS10 are members of the D/R12 family. RGS14 is a complex multidomain signaling molecule selective for Gαi/o (Cho et al., 2000; Vellano et al., 2011) and is highly expressed in brain regions essential for learning and memory (Harbin et al., 2021). RGS10 is a smaller molecule that selectively binds Gαi/o members (Hunt et al., 1996; Watson et al., 1996; Popov et al., 1997). In contrast to RGS14, RGS10 is broadly expressed making it an essential regulator of physiologic processes including inflammatory responses and survival signaling (Alqinyah et al., 2018). Much smaller than RGS14, RGS4 is part of the R4 subfamily and is highly expressed in brain where it has been linked to psychiatric disorders (Terzi et al., 2009; Schwarz, 2018), and in opioid reward and addiction (Sakloth et al., 2020). RGS4 is selective for Gαi/o and Gαq members (Hepler et al., 1997; Tesmer et al., 1997), preferring signaling by Gαi/o over Gαq in a neuronal model (Masuho et al., 2020).

In the present study, we carry out a functional assessment of the predictive capabilities of the novel 3DMTR applied to RGS proteins. We combine this with available somatic mutational information found in cancer samples to determine the effect these genetic variants will have on RGS14/10/4 protein structure and function. We test how cancer mutations in significant regions of the protein can lead to changes in RGS function assessed by various cell based and biochemical assays.

Materials and Methods

Three-Dimensional Missense Tolerance with Permutation Analysis. The 3DMTR permutation analysis was performed as described (Perszyk et al., 2021). To perform 3DMTR analysis on RGS protein structures, the encapsulated application MATLAB (Mathworks, version R2019b) available on GitHub (https://github.com/riley-perszyk-PhD/3DMTR, current version v2.000) was used. The protein structures of the analyzed RGS proteins were obtained from the Protein Data Bank (rcbs.org). Reference of all the crystal structures used is available in Supplemental Table 1. Variant datasets of all RGS genes were downloaded from the Genome Aggregation Database (gnomAD) website (https://gnomad.broadinstitute.org/, version 2.1.1). The translated coding gene sequences of RGS proteins were used (RGS1, NM_002922.4; RGS2, NM_002923.4; RGS3, NM_144488.6; RGS4, NM_001102445.2; RGS5, NM_003617.4; RGS6, NM_001204416.3; RGS7, NM_001282773.2; RGS8, NM_033345.3; RGS9, NM_001081955.3; RGS10, NM_001005339.2; RGS12, NM_002926.3; RGS14, NM_006480.5; RGS16, NM_002928.4; RGS17, NM_012419.5; RGS18, NM_130782.3). The closest 21 residues were used in the 3DMTR calculations since the RGS protein domain structures are small (~120 residues) to provide more stratified scores. Permutation analysis was preformed using 1000 iterations by randomizing the residue location. Permutation significance was determined where the 3DMTR score was outside the 2xSTD range (permutation standard deviation of each residue) calculated from the permutation mean score for each residue. We define the residues that are identified with permutation analysis as either significantly intolerant or significantly tolerant depending on which tail of the permutation distribution they fall within. Additionally, having an MTR score of <0.5 is very rare (the fifth percentile score for the 1DMTR is 0.5462; http://mtr-viewer.mdhs.unimelb.edu.au/). Previous work suggests that the 3DMTR and the 1DMTR generally produce a similar set of MTR scores, albeit the scores are rearranged based on the different selection criteria, so we believe this cut off is also appropriate for the 3DMTR scores. Thus, we deem the residues with 3DMTR scores ≤ 0.5 as being important and will call highly intolerant.

Cell Culture and Reagents. Human embryonic kidney (HEK) 293 cells were cultured in 1X Dulbecco's modified Eagle's medium (DMEM), without phenol red indicator, supplemented with 10% fetal bovine serum (FBS), 2mmol/l L-glutamine, 100 units/ml penicillin, and 100 mg/ml streptomycin. HEK cells were kept in a humidifier incubator with 5% CO_2 at 37°C. Trypsin-EDTA 0.25% was used during cell culture procedures. Cells were seeded $8x10^5$ in 2 ml of transfection medium per well in six-well plates. Transfection media was formulated with 5% FBS in DMEM phenol-red free media and polyethyleneimine (PEI) was the transfection agent used.

The hemagglutinin (HA) epitope-tagged α2a-adrenergic receptor (HA-α2a-AR) construct was kindly provided by Dr. Joe Blumer (Medical University of South Carolina). The G protein used in our studies were Glu-Glu tagged Gαo (Gαo-EE) and the pertussis-resistant mutant C351G of Gαo (Gαo-CG) which was purchased from the cDNA Resource Center (cDNA.org, Bloomsberg, PA). Mas-GRK3ct-Luc and Ven-Gβγ were described previously (Hollins et al., 2009). Human Flag-tagged RGS14 [Flag-RGS14 wild-type (WT)], human Flag-RGS14-S127P, human Flag-RGS14-D137Y, human Flag-RGS14-R173C, human Flag-RGS14-R173H, human Flag-tagged RGS10 wild-type (Flag-RGS10

WT), human Flag-RGS10-S64T, human Flag-RGS-K89M, hemagglutinin epitope-tagged rat RGS4 wild-type (HA-RGS4 WT), rat HA-RGS4-K125Q, rat HA-RGS4-E126K, and rat HA-RGS4-E135K were generated as previously described (Bernstein et al., 2004; Shu et al., 2007). Pertussis toxin #181 was purchased from List Biologic Laboratories, Inc (Campbell, CA). UK 14,304 was obtained from Sigma-Aldrich (U104; St. Louis, MO). Forskolin was obtained from Sigma-Aldrich (F6886; St. Louis, MO).

Kinetic Bioluminescence Resonance Energy Transfer. Kinetic bioluminescence resonance energy transfer (BRET) experiments were performed as previously described (Lambert et al., 2010; Brown et al., 2016). After a 48-hour transfection, cells were resuspended in Tyrode's solution (140 mmol/l NaCl, 5 mmol/l KCl, 1 mmol/l $MgCl_2$, 1 mmol/l $CaCl_2$, 0.37 mmol/l NaH_2PO_4, 24 mmol/l $NaHCO_3$, 10 mmol/l HEPES, and 0.1% glucose, pH 7.4) and plated on white 96-well Optiplates (Perkin Elmer Life Sciences, Waltham, MA). Fluorescence measurements were made using the TriStar LB 941 plate reader (Berthold Technologies, Bad Wildbad, Germany) with 485-nm excitation and 530-nm emission filters to confirm acceptor expression. After a 10-minute application of 5 μmol/l coelenterazine H (Nanolight Technologies, Pinetop, AZ), in vivo kinetic BRET was recorded using sequential measurements through 485- and 530-nm emission filters. BRET was recorded for 30 seconds with no stimulation to establish basal BRET. After 30 seconds of basal BRET recording, α2A-adrenergic receptor agonist UK 14,304 (100 μM) was injected into the cells. The presence of the agonist induces Gα protein activation and the change in BRET is calculated by dividing the mas-GRK3ct-Luc signal (530 nm) by the Ven-G$\beta\gamma$ signal (485 nm) and subtracting the average BRET signal observed from the first 30 seconds of observation (basal BRET). With each experiment, a kinetic BRET control was performed using pertussis insensitive Gαo. Pertussis toxin was added to the transfection media to all wells. Any BRET signal recorded in the control wells transfected with pertussis sensitive Gαo was regarded as noise and subtracted from experimental kinetic BRET recordings. Data were collected using the MikroWin 2010 software (Mikrotek Laborsysteme GmbH, Overath, Germany) and analyzed using Microsoft Excel and GraphPad Prism 9.

Coimmunoprecipitation of RGS and Gαo. After a 24-hour transfection, HEK cells were washed three times with cold 1X PBS. Cells were scraped into AMF lysis buffer (50 mM Tris, 150 mM NaCl, 1 mM EDTA, 2 mM DTT, 10 mM NaF, 14 mM $MgCl_2$, 10 mM $AlCl_3$, 1X Roche protease inhibitor, 1X Halt phosphatase inhibitor) and lysed at 4°C for 1 hour while rotating end-over-end. Lysates were cleared by centrifuging at 13000 RPM for 10 minutes at 4°C. For each condition, 50 μl of affinity gel beads was used. Anti-FLAG M2 affinity gel (Sigma A2220) was used to immunoprecipitated Flag-RGS14 and Flag-RGS10, while monoclonal anti-HA agarose beads (Sigma A2095) was used for HA-RGS4 immunoprecipitations. Affinity gel beads were washed three times with cold 1X PBS and then blocked with 4% BSA in PBS at 4°C for 1 hour while rotating end-over-end. Cleared cell lysate was collected for input, and the remaining lysate was added to blocked anti-FLAG M2 affinity beads or anti-HA agarose beads. Immunoprecipitation of Flag-tagged RGS from lysate was performed at 4°C for 2 hours while rotating end-over-end, while HA-tagged RGS was performed overnight. After immunoprecipitation, the beads-RGS complex was washed three times with cold 0.1% Tween-20 in PBS. Input and immunoprecipitated samples were denatured by boiling in Laemmli buffer for 5 minutes.

Analysis of Immunoblots. Denatured cell lysate samples in Laemmli Buffer were resolved on 13.5% SDS-PAGE, and samples were then transferred to nitrocellulose membranes. Membranes were blocked in 5% non-fat milk for 1 hour at room temperature. For FLAG-tagged RGS (RGS10 WT and mutants, or RGS14 WT and mutants.), HRP-conjugated anti-FLAG antibody (Sigma A8592, 1:15,000) was diluted in TBS/T and incubated with the membranes for 45 minutes at room temperature. For HA-tagged RGS4 and mutants, Anti-HA-Peroxidase rat monoclonal antibody (Roche Cat# 12013819001, 1:5000) diluted in TBS/T was used. For Gαo, anti-EE (Covance MMS-115R, 1:1000) was diluted in 5% non-fat milk and incubated with membranes overnight at 4°C. HRP-conjugated goat anti-mouse IgG secondary antibody (Jackson ImmunoResearch 115-035-003, 1:5000) was diluted in TBS/T and incubated with membranes for 45 minutes at room temperature. Blots were developed using ECL and imaged using the Chemi-Doc MP Imaging system (BioRad).

GloSensor cAMP Assay. To measure intracellular cAMP levels, we used the GloSensor cAMP assay. The cAMP GloSensor was obtained from Promega and the assay was performed following the manufacturer's instructions (Promega, Madison, WI, USA). HEK293 cells were harvested (15,000 cells per individual well) in tissue culture-treated 96-well flat bottom plate. Cells were kept in 37°C tissue culture incubator 5%–10% CO_2 overnight. Cells were transfected with 50ng of pGloSensor-20F cAMP, 50ng α2-AR, 50ng RGS of interest, and pcDNA in DMEM serum free media. After 24 hours, the media is removed without disrupting the cell monolayer and 100 μl of the equilibrium medium is added (2% v/v dilution of the GloSensor cAMP Reagent stock solution). Incubation with the equilibration reagent is done for 2 hours and cells are kept in 37°C tissue culture incubator 5%–10% CO_2 in the dark. After 2 hours, basal luminescence intensity was measured at 0 and at 5 minutes using a luminometer (FLUOstar) in triplicates. To measure α2-AR-Gαi/o directed inhibition of cAMP, cells are preincubated with 100 μl of 100 μM UK14,304 (agonist) or DMSO (vehicle) in HBSS for 10 minutes at room temperature following basal readings. At 10 minutes, cAMP production is stimulated by adding 10 μM forskolin and luminescence is measured every 5 minutes for a total of 50 minutes. The data in relative light units (RLU) from triplicates wells were averaged and a response over time graph is generated. Normalization was done by dividing each time point following forskolin stimulation over basal luminescence, then each time point is divided by empty vector (50ng pcDNA alone) control. Area under the curve for each condition is calculated and the effect of the mutants is compared with the WT RGS effect in Gαi/o-coupled α2-AR stimulation of cAMP.

Data Analysis and Statistics. Data analysis was conducted using Microsoft Excel and GraphPad Prism 9 software. Kinetic BRET activation curves were presented as a mean of three or four experimental replicates. We then selected the maximum BRET amplitude at 100 seconds for each condition. Maximum BRET amplitude columns were compared by performing a statistical analysis using one-way analysis of variance (ANOVA) with Dunnett's test. Luminescence-based cAMP GloSensor assay relative light units (RLU) were recorded from averaged replicate wells and plotted as response over time, with a total of 4 experimental replicates. We then analyzed the area under the curve (AUC) for each condition and columns were statistically analyzed using one-way analysis of variance (ANOVA) with Dunnett's test.

Results

3DMTR Predicts Amino Acid Residues in RGS Proteins Likely To Be Intolerant to Mutation. RGS proteins share an evolutionary conserved ~120 amino acid RGS domain that binds activated G protein alpha subunits to act as GAPs. In this study, we examined the canonical human RGS proteins using a bioinformatic tool that evaluates the degree of variation that exists in the gnomAD database (large database of human whole exomes and genomes of healthy individuals) and determines a composite score, missense tolerance ratio (MTR) (Traynelis et al., 2017). This MTR score is determined based on the location of the linear polypeptide chain (1DMTR; Traynelis et al., 2017). A newly described bioinformatics tool expands on this idea to measures MTR based on the location of each residue in three-dimensional (3D) space (3DMTR;-Perszyk et al., 2021-) based on reported protein crystallography or cryo-EM data. This 3DMTR is a more

accurate and improved bioinformatic tool that also utilizes a permutation analysis to calculate the relative significance of the missense tolerance ratio of a given dataset (Perszyk et al., 2021). Both 1DMTR and 3DMTR use available human variation data from neighboring residues to report population level genetic variation and measures the tolerance ratio within the entire genome.

A comparison of the 1DMTR and the 3DMTR analysis for the RGS domain of one representative RGS protein, RGS14, is shown as scatter plots in Fig. 1, A and C. In a previous report (Squires et al., 2021), we described in detail the 1DMTR results for RGS proteins. Considering the RGS domain of RGS14 (Fig. 1A), the 1DMTR analysis of the RGS domain generally shows more tolerant scores (0/134 residues have 1DMTR scores ≤0.5), which are shown as red shades superimposed onto the RGS domain structure (Fig. 1B). Structural data has been reported for the RGS domain of most RGS proteins, including RGS14 (Soundararajan et al., 2008). Using this information, we analyzed the RGS domains of 15 of 20 RGS protein family members, including RGS14, using the 3DMTR analysis (Supplemental Fig. 1) as will be discussed further below. In contrast to 1DMTR, the 3DMTR uses the same human variation data but instead utilizing the neighboring residues in 3D space, which should be functionally more relevant to determine the tolerance ratio.

We analyzed the RGS domain of RGS14 by 3DMTR (Fig. 1, C and D). Because the size of RGS domains (~120 aa) are much smaller than the entire RGS proteins (~200–1400 aa), the 3DMTR was calculated using the nearest 21 residues instead of the 31-residue window that has been used for larger proteins. Based on this, the 3DMTR may be a more accurate predictor of highly intolerant residues compared with the 1DMTR. We will refer to the residues that appear to have selective pressure controlling their variation as 'highly intolerant' (3DMTR score of ≤0.5). The 3DMTR analysis of the RGS domain of RGS14 identified several residues with highly intolerant scores (7/134 residues have 3DMTR scores ≤0.5, Fig. 1C), shown in blue shades superimposed onto the RGS domain structure (Fig. 1D). Furthermore, we used permutation analysis that determines which residue scores are highly unlikely given a specific dataset (occurring in

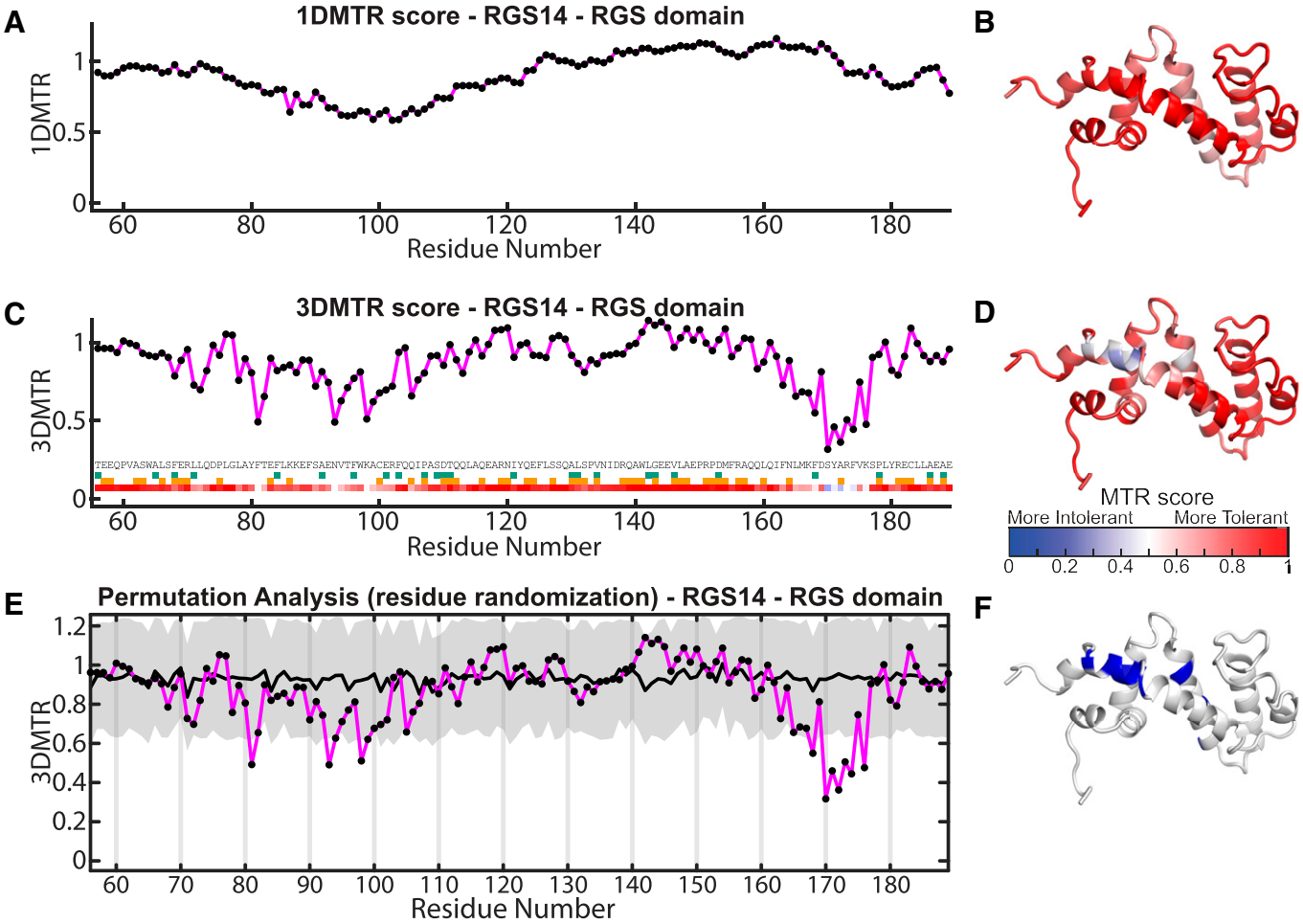

Fig. 1. Comparison of RGS14 1DMTR and 3DMTR permutation analysis. (A) The sequential MTR score of RGS14 (31 residue smoothing window) is calculated using gnomAD-derived human variants and is shown as a scatter plot. (B) Structural view of RGS domain of RGS14 colored to show a heatmap of the 1DMTR score (intolerant residues in blue, neutral in white, tolerant in red). (C) The MTR score of RGS14 taking into consideration three-dimensional space (3DMTR; using the closest 21 residues). Green squares represent a synonymous variant in that residue. Orange squares represent missense variant for the residue. Below is a linear heatmap of the MTR score for RGS14. (D) Structural view of RGS14 3DMTR raster plot scores. (E) Scatter plot of RGS14 3DMTR score (magenta line), permutation analysis score mean (black line), and 2× standard deviation around the permutation score mean of the permutation analysis (gray areas). (F) Structural view of the permutation analysis raster plot significantly intolerant residues within RGS14.

less than 5% of random permutations). It can be interpreted that the residues identified by permutation analysis that are either significantly intolerant or significantly tolerant, i.e., those that would be unexpected within each analyzed dataset (consisting of the gene sequence, protein structure, and gnomAD dataset). Primarily of note, the analysis suggests that the significantly intolerant residues may relatively (compared with the rest of the residues in the protein) have selective pressures that limit variation in these regions. The permutation analysis of RGS14 (Fig. 1E) identified 14 residues that were significantly intolerant, whereas 3.4 would have been expected randomly given the dataset (based on the expected frequencies of a single tail of a normal distribution using α equal to 0.05, therefor 0.025 * 134 residues). Comparing the 1DMTR and 3DMTR data for RGS14, the 3DMTR analysis of the RGS domain of RGS14 predicts highly intolerant residues not found with the 1DMTR (0 with 1DMTR versus 7 with 3DMTR, total residues 134, Fisher's exact test $P = 0.0144$). The permutation analysis of RGS14 (Fig. 1E) identified 14 residues significantly intolerant, seven residues highly intolerant (3DMTR score ≤ 0.5) and seven tolerant (not highly intolerant) (3DMTR score >0.5). The significantly intolerant residues are visualized in blue on the structure of the RGS domain of RGS14 (Fig. 1F).

Next, each RGS domain of all available structures for RGS protein family members were analyzed using 3DMTR (Fig. 2; Supplemental Fig. 1). For this analysis, we used the reported structures of RGS protein domains that are available for 15 of the 20 RGS proteins (Supplemental Fig. 1). Interestingly, each RGS domain presented a distinct "bar code" of significantly intolerant and significantly tolerant residues (Fig. 2; Supplemental Fig. 1). A second 3DMTR analysis was performed on four RGS protein domains in complex with active forms of their Gα partners (Supplemental Fig. 2: RGS1-Gαi1, RGS4-Gαi1, RGS10-Gαi3 and RGS16-Gαi1). In each of these cases, the profiles for significantly tolerant and intolerant residues differed slightly by active Gα binding.

We next compared the 3DMTR results for RGS14, RGS10 and RGS4. These three RGS proteins were chosen because of their involvement with various cancers and their differences in size and structure. Raster plots for RGS14 (Fig. 2A), RGS10 (Fig. 2B), and RGS4 (Fig. 2C) show the comparison of 1DMTR data with 3DMTR data calculated using the nearest 21 or 31 residues, as before. For each, tolerant (red) or significantly intolerant (blue) residues are shown (c21-sig). The 3DMTR analysis predicts intolerant residues not found with the 1DMTR analysis. As observed with the other RGS proteins (Supplemental Fig. 1), the RGS domains of RGS14, RGS10, and RGS4, each presented a distinct "bar code" of significantly intolerant residues (Fig. 2; Supplemental Figs. 1 and 2).

As was the case for RGS14 (Figs. 1 and 2A), 3DMTR predicted for RGS10 more highly intolerant scores than 1DMTR (Fig. 2B) (1 with 1DMTR versus 7 with 3DMTR, total residues 136, Fisher's exact test $P = 0.0663$) and for RGS4 (Fig. 2C) (1 with 1DMTR versus 6 with 3DMTR, total residues 128, Fisher's exact test $P = 0.1199$). The structure of each of the RGS domains is shown with significantly tolerant and intolerant residues highlighted in red and blue, respectively (Fig. 2, D–I). Each is shown bound to the reported structure of Gαi1 (Fig. 2, D and F), Gαi3 (Fig. 2E), or alone (Fig. 2, G–I). Comparison of the three RGS domain structures in the same orientation with the intolerant residues highlighted in blue (Fig. 2, G–I), shows that these residues are distributed differently within the domain structure. We next performed permutation analysis for the RGS domains of RGS10 and RGS4 (Supplemental Fig. 3) and compared those to RGS14 (Fig. 1E).

The amino acid sequence for each of these RGS proteins are aligned (Fig. 2J). The RGS domain is highlighted in lilac, in gray are the residues that directly interact with Gα, and in orange the residues that are in the hydrophobic core (Tesmer et al., 1997). The significant residues identified by the permutation analysis are identified with symbol under each residue letter, * for the identified residues that were also highly intolerant (MTR $\leq$ 0.5) and ^ for identified residues that were not highly intolerant residues (MTR $>$0.5). As shown in Fig. 2J, the profiles of intolerant residues differ across each protein. 3DMTR identified highly intolerant residues found in the RGS hydrophobic core were residue F81 in RGS14, and I93 and F97 in RGS10. 3DMTR identified highly tolerant residues in RGS4 F91, W92 and I114 are also found in the hydrophobic core. Intolerant residues in the direct contact with G alpha in RGS14 are N93 and R173, and tolerant residues are RGS14-D137 and RGS4 E87 and N88. Compared with the permutation analysis for RGS14 (Fig. 1E), the same analysis of RGS4 identified 15 significantly intolerant residues, whereas 3.2 would have been expect randomly given the 128-residue dataset. The permutation analysis of RGS10 identified five residues that were significantly intolerant, whereas 3.4 would have been expected randomly given the 136-residue dataset.

We next focused on the significantly intolerant or tolerant residues in RGS14, RGS10 and RGS4 identified by the 3DMTR analysis that overlap with reported somatic pathogenic mutations found in patient cancer samples identified in the Catalogue of Somatic Mutations in Cancer (COSMIC) database (Table 1). Using various in vitro assays of RGS-G protein interaction and signaling, we test the effect of an amino acid change, due to cancer mutations, in the selected significant residues and how these affect canonical RGS function.

Reported Pathogenic Somatic Mutations in RGS14, RGS10, and RGS4 That Overlap with Residues Identified by 3DMTR To Be Significantly Intolerant to Mutation. Several bioinformatics tools (discussed below) that estimate the pathogenic potential of reported human somatic mutations are publicly available. Cells can develop somatic mutations due to imperfect replication or exposure to endogenous and exogenous mutagens (Olafsson and Anderson, 2021). Most somatic mutations will have little or no phenotypic effect, whereas a small minority of mutations can affect protein function and cell physiology leading to the progress of complex diseases (Olafsson and Anderson, 2021). These mutations occur postzygotically and exist in a subpopulation of cells (Dou et al., 2018). Online databases like COSMIC (cancer.sanger.ac.uk/cosmic) report somatic mutations found in human cancers. COSMIC uses a FATHMM-MKL algorithm to predict the functional, molecular and phenotypic consequences of proteins missense variants using Markov models classifying the mutations as pathogenic (scores $\geq$ 0.7) or neutral ($\leq$0.5) (Shihab et al., 2015; Tate et al., 2019). Using these tools, we identified somatic mutations that overlap with residues in the RGS domain of RGS14, RGS10 and RGS4 identified by the 3DMTR to be either more sensitive or less sensitive to mutations (Supplemental Tables 2–4).

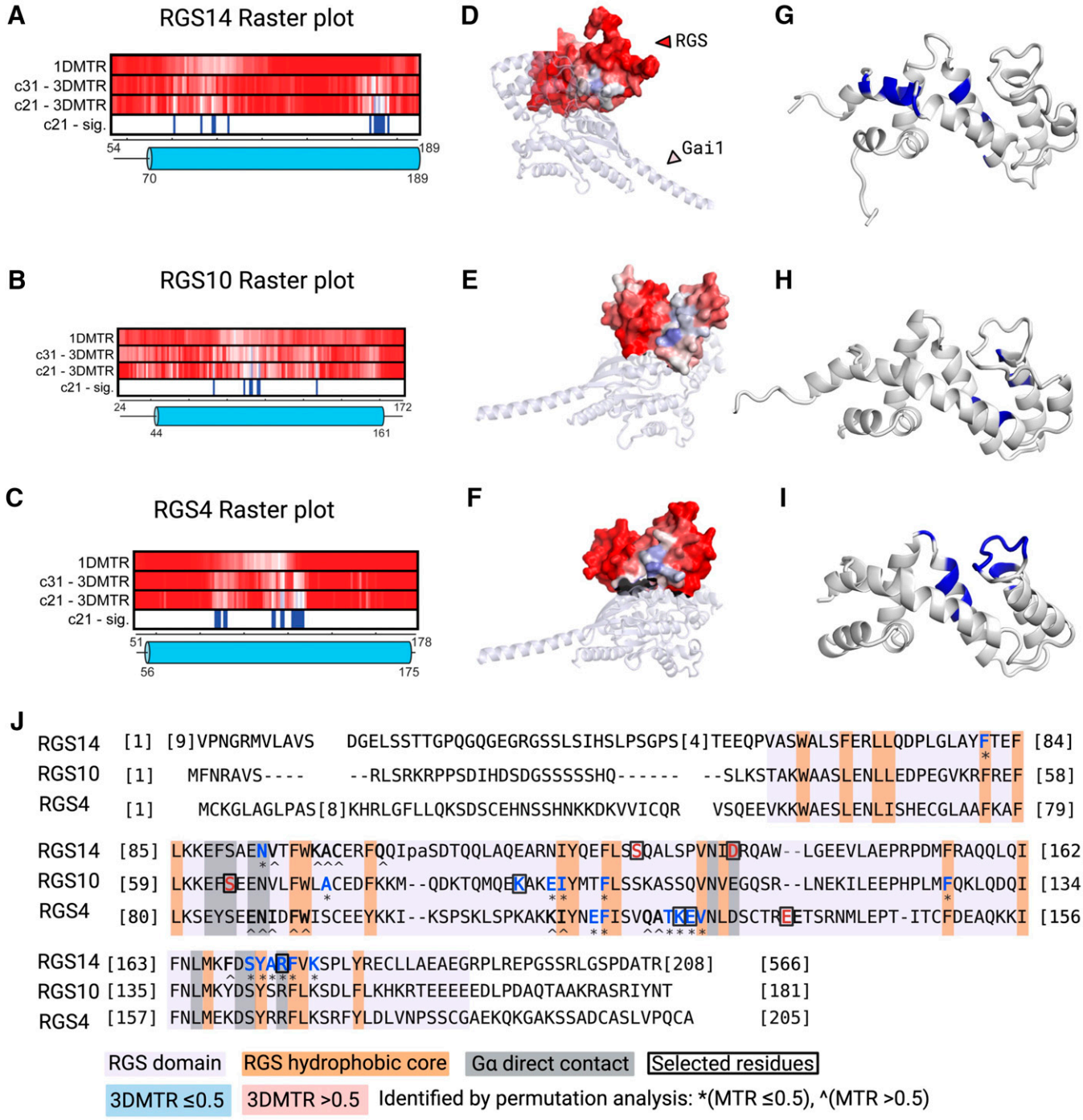

Fig. 2. The 3DMTR permutation analysis identifies significantly intolerant residues within the RGS domain that were not identified by 1DMTR. (A–C) Raster plot of selected RGS proteins comparing 1DMTR, 3DMTR based on the 31 neighboring residues, 3DMTR based on the 21 neighboring residues, and significantly intolerant residues based on the permutation analysis (rows labeled "c21-sig.", labeled by a blue rectangle). (D–F) Structural views of RGS domains colored to show a heatmap of the 21-residue 3DMTR score (intolerant residues in blue, neutral in white, tolerant in red) bound to G alpha. (G–I) Structural view of the 21-residue 3DMTR permutation analysis raster plot significantly tolerant/intolerant residues. (J) RGS protein alignment shows the RGS domain (lilac), residues in the hydrophobic core (yellow), residues in direct contact with G alpha (gray), and selected residues to test the functional consequences inside box. The residues with a 3DMTR score >0.5 are determined to be not highly intolerant (tolerant) and the color letter is red. Residues with a 3DMTR score ≤0.5 are determined to be highly intolerant and the color letter is blue. Residues identified via the permutation analysis are identified with symbols * (MTR ≤ 0.5, highly intolerant) or ^ (MTR > 0.5, not highly tolerant).

RGS14 has been reported to be highly expressed in liver cancer and glioma (Uhlen et al., 2017). The analysis of The Cancer Genome Atlas (TCGA) and Gene Expression Omnius (GEO) datasets have identified RGS14 as one of the five-gene signature biomarkers for Glioblastoma for Glioblastoma multiforme (GBM) (Yin et al., 2019). Somatic mutations in RGS14 that overlap with residues predicted to be highly tolerant or intolerant by the 3DMTR are shown in Supplemental Table 2. Mutations found in RGS14 of patient samples with large intestine carcinoma include R173C, R173H, and S170R.

TABLE 1
Tolerant and intolerant residues from RGS domains of interest that also overlap with highly deleterious somatic mutations were selected for assessment of their impact on RGS functions. Amino acids reported in the COSMIC cancer database were selected based on the criteria that were predicted to be pathogenic by the FATHMM score to be highly pathogenic. Scores above 0.5 are deleterious; scores ≥0.7 are classified as pathogenic.

	Pathogenic Score	Cancer Type	3DMTR (Score)
RGS14			
S127P	0.91	Stomach Carcinoma	Tolerant (1.03)
D137Y	0.97	Prostate Carcinoma	Tolerant (0.93)
R173C	0.81	Large Intestine Carcinoma	Intolerant (0.50)
R173H	0.97	Large Intestine Carcinoma	Intolerant (0.50)
RGS10			
S64T	0.96	Lung Carcinoma	Tolerant (0.91)
K89M	0.84	Thyroid Carcinoma	Intolerant (0.48)
RGS4			
K125Q	0.97	Lung Adenocarcinoma	Intolerant (0.48)
E126K	1.00	Skin Melanoma	Intolerant (0.42)
E135K	1.00	Skin Carcinoma, Melanoma, Upper Aerodigestive Tract Carcinoma	Tolerant (1.14)

RGS14 somatic mutation S127P is found in gastroesophageal junction carcinoma, and D137Y is found in prostate carcinoma. Of note, coding silent mutations in RGS14 and other RGS proteins are also reported that overlap with the residues identified by 3DMTR permutation analysis (significantly intolerant residues). For RGS14 these are residues N93, A99 and R173, and are included because the COSMIC FATHMM-MKL algorithm surprisingly and inexplicably designated some of these silent mutations to be pathogenic. Residues in RGS14 scored by the 3DMTR permutation analysis (>0.05) and overlap with somatic mutations considered pathogenic by the COSMIC algorithm are S127P and D137Y. Residues scored by the 3DMTR permutation analysis (≤0.05, significantly intolerant residues) and predicted to be pathogenic are S170R, R173C, R173H, and coding silent R173.

RGS10 has been reported to be highly expressed in renal, endometrial, and cervical cancer (Uhlen et al., 2017). This ubiquitously express protein regulates physiology and signaling pathways in microglia, macrophages, T-lymphocytes, neurons, osteoclasts, cardiomyocytes, platelets, and cancer cells. It has been identified as an important regulator of cell survival and chemoresistance (Hooks et al., 2010; Cacan et al., 2014) and transcript expression is significantly suppressed in multiple ovarian cancer cell lines (Ali et al., 2013; Cacan et al., 2014). Moreover RGS10 acts as a tumor suppressor by blunting endogenous survival pathways (Cacan et al., 2014), and has been reported to regulate inflammatory signaling pathways in ovarian cancer cell survival (Alqinyah et al., 2018). Somatic mutations in RGS10 that overlap with residues deemed to be highly tolerant or intolerant by the 3DMTR are shown in Supplemental Table 3. Mutations found in RGS10 of patient samples with lung carcinoma are S64T and coding silent A73, while K89M can be found in thyroid carcinoma samples.

Studies have shown association between RGS4 and enhanced cell viability, invasion and motility in thyroid cancer (Nikolova et al., 2008), glioma (Tatenhorst et al., 2004; Weiler et al., 2013), ovarian cancer (Puiffe et al., 2007), and triple negative breast cancer (Xie et al., 2009). Somatic mutations in RGS4 that coincide with 3DMTR permutation analysis identified significant residues (Supplemental Table 4) are found in carcinoma samples of the following tissues: large intestine E87D, thyroid I89N, kidney W92C, endometrium K113N, breast Q122H and A123E, stomach A123T, and lung K125Q. Overlapping mutants were also found in melanoma including E126K, E135K, and silent coding F118 and V127 in RGS4.

Based on these findings, we chose to study selected somatic mutations in RGS14, RGS10 and RGS4 that overlap with residues identified by 3DMTR to be either tolerant or intolerant to mutation. Our goal for these studies was to test how well 3DMTR and other bioinformatic tools predict important residues for protein function and pathogenic potential. These specific residues and somatic mutations chosen for further study are listed in Table 1. Mutations in RGS14 selected for study were S127P, D137Y, R173C, and R173H (Fig. 3). Mutations in RGS10 selected for further study are amino acid mutation S64T and K89M (Fig. 4). Mutations in RGS4 chosen for further study were K125Q, E126K, and E135K (Fig. 5).

Assessment of Somatic Mutations in 3DMTR-Identified Tolerant and Intolerant Residues in GPCR/G Protein Activation and G Protein Binding. RGS14 is a member of the D/R12 subfamily and contains an RGS domain as well as accessory domains that play a role in different signaling pathways such as the tandem Ras/Rap-binding domains (R1 and R2), a G protein regulatory (GPR) motif, and a C-terminal PDZ binding motif (Cho et al., 2000; Traver et al., 2000; Hollinger et al., 2001; Hollinger and Hepler, 2002; Shu et al., 2007; Vellano et al., 2013; Zhao et al., 2013; Friedman et al., 2022). We first examined the effects of mutational changes in 3DMTR-defined tolerant and intolerant residues on RGS14 functions (Fig. 3). For these and subsequent studies (Figs. 4 and 5), we used a live cell biosensor (BRET) assay to measure RGS effects on GPCR/G protein activation (Brown et al., 2016). HEK293 cells were transfected with α2A-adrenergic receptor (α2AR), Gαo, Gβ1-venus, Gγ2-venus, and the biosensor for Gβγ binding mas-GRK3ct-Luc, as previously reported (Brown et al., 2016). Upon addition of α2AR agonist UK 14,304 (100μM), GPCR signaling is activated leading to the dissociation of Gα and Gβγ-venus. The Gβγ-venus binds to the mas-GRK3ct-Luc biosensor resulting in

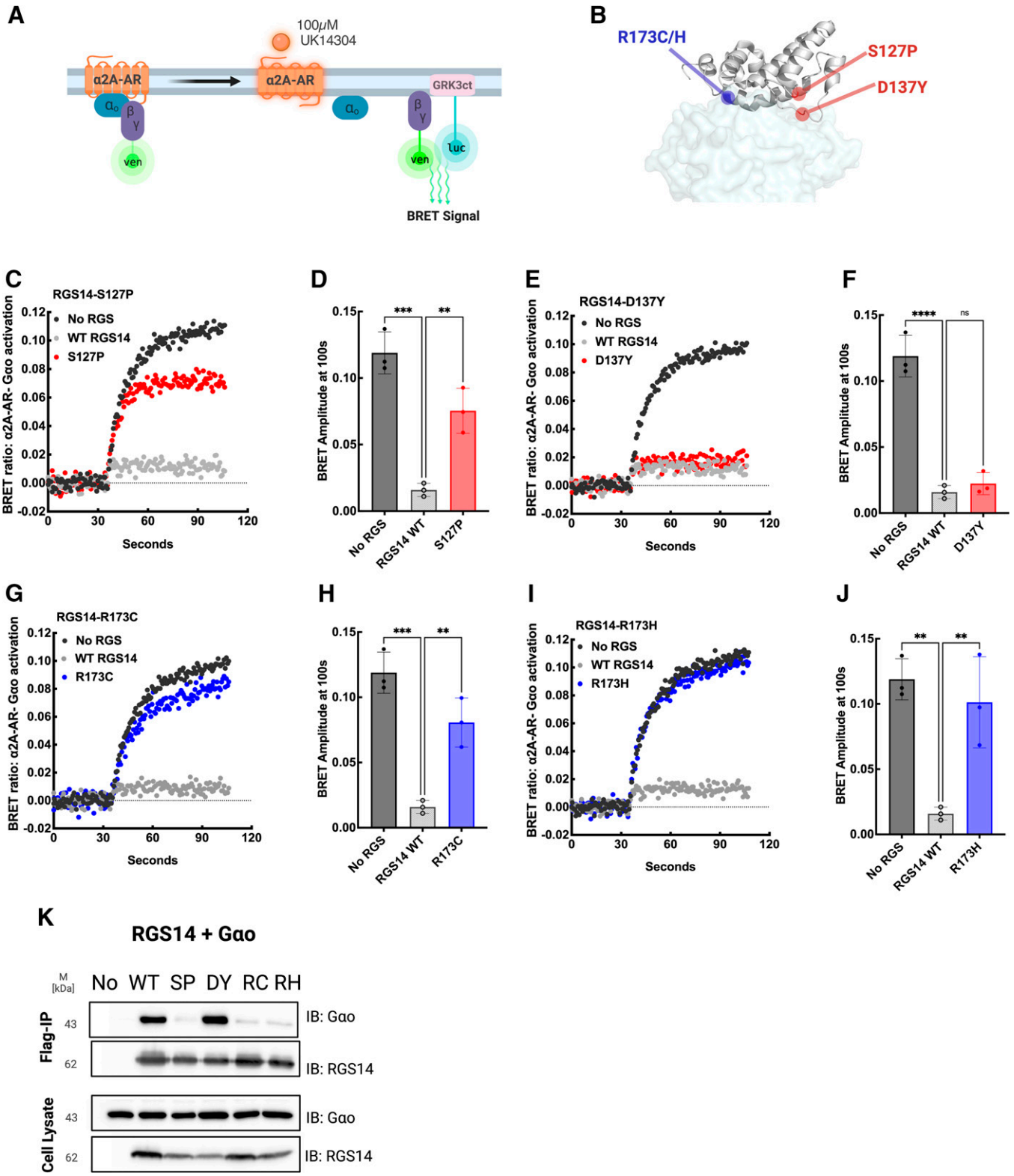

Fig. 3. Assessment of functional impact of RGS14 somatic mutations on GPCR-G protein activation and G protein binding. (A) Schematic representation of kinetic BRET experiments. HEK 293 cells were transfected with 200 ng of α2A-AR, 200 ng of Venus-Gβ1 200 ng of Venus-Gγ2, 200ng of mas-GRK3ct-Luc, 1000 ng of mutant Gαo (PTX insensitive), and 0 or 200ng of WT Flag-RGS or 200ng of Flag tagged RGS mutant. (B) Structural view of selected mutated tolerant (red) and intolerant (blue) residues in RGS14. Average whole traces of BRET signal over time (n = 3) are shown comparing WT and somatic mutations. 3DMTR identified residues that led to loss of function are tolerant residues Flag-S127P (C), and intolerant mutated residues Flag-R173C (G) and Flag-R173H (I). Tolerant residue Flag-D137Y (E) did not lead to change of function. BRET amplitude observed at 100s was compared between 0ng RGS14, 200ng WT RGS14, and mutants Flag-S127P (D), Flag-D137Y (F), Flag-R173C (H), and Flag-R173H (J). Error bars represent mean ± S.D. Statistical analysis was performed using one-way ANOVA with Dunnett's test (**$P < 0.005$). (K) Coimmunoprecipitation studies show that RGS14 mutants S127P, R173C and R173H blocked binding to Gαo-AlF4.

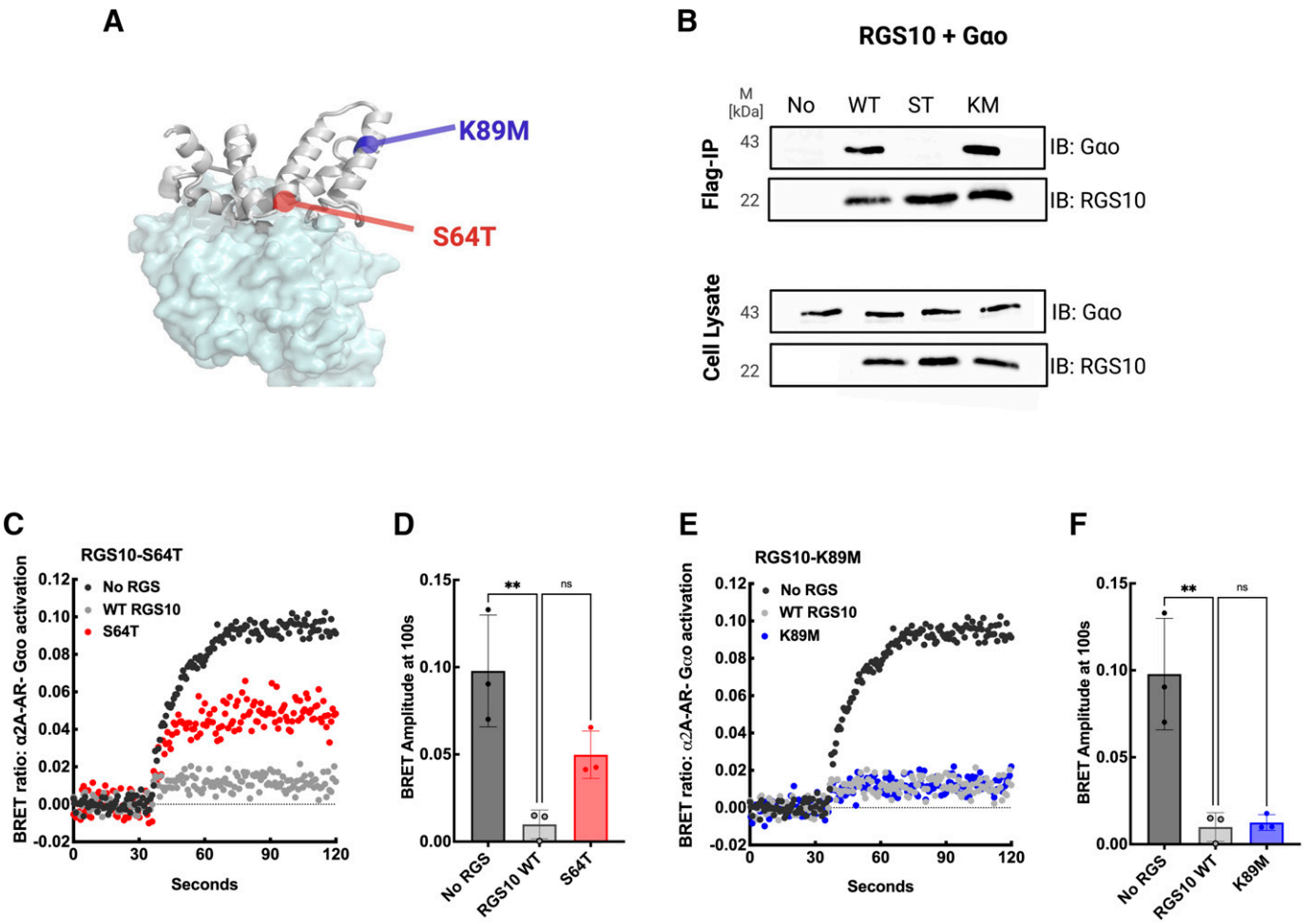

Fig. 4. Assessment of functional impact of RGS10 somatic mutations on GPCR-G protein activation and G protein binding. (A) Structural view of selected mutated tolerant (red) and intolerant (blue) residues in RGS10. (B) Coimmunoprecipitation studies show that mutants K89M bound to Gαo-AlF4$^-$ while S64T blocked binding. Average whole traces of BRET signal over time (n = 3) are shown comparing WT and 3DMTR somatic mutations in identified tolerant residue Flag-S64T (C) and intolerant residues Flag-K89M (E). BRET amplitude observed from data presented for Flag-S64T (D) and Flag-K89M comparison (F). Tolerant residue Flag-S64T (C–D) led to change of function while intolerant Flag-K89M (E–F) did not change. Error bars represent mean ± S.D. Statistical analysis was performed using one-way ANOVA with Dunnett's test (**$P < 0.005$).

an increase in BRET signal (Hollins et al., 2009). Using this model (Fig. 3A) we can test the effects of RGS mutants in α2-adrenergic receptor-Gαo protein activation.

RGS4, RGS10 and RGS14 each bind to active Gαi/o protein family members including Gαo1, Gαo2, Gαi1, Gαi2, and Gαi3 (Masuho et al., 2020). Of these, Gαo is the most indiscriminate G alpha protein, is regulated by all canonical RGS proteins (Masuho et al., 2020), and its highly expressed in the brain where it couples α2AR (Nobles et al., 2005; Goldenstein et al., 2009). Our previous studies compared α2AR G protein activation with Gαo and Gαi1, and Gαo provided a much more robust maximum BRET amplitude signal (Brown et al., 2016). For these reasons, we employed a live cell α2AR-Gαo model to test the effects of RGS protein mutants in G protein activation.

Using the above assay, we examined the effects of selected somatic mutations on RGS14 capacity to regulate receptor-G activation (Fig. 3). Four mutations were tested including two that were scored by 3DMTR-permutation analysis as tolerant (S127P and D137Y) (Fig. 3, C–F) and two as intolerant (R173C and R173H) (Fig. 3, G–J). Wild-type RGS14 and mutant proteins expressed well in HEK 293 cells (Supplemental Fig. 4A). The relative position of these residues within the RGS domain structure are shown in Fig. 3B highlighted as either red (tolerant) and blue (intolerant). As shown in Fig. 3, C–F, somatic mutations within the tolerant residues exhibited distinct phenotypes. Whereas mutant D137Y behaved as expected (i.e., like wild-type RGS14) to inhibit agonist activation of α2AR-Gαo (Fig. 3, E and F), mutant S127P exhibited a loss-of-function (LoF) phenotype (Fig. 3, C and D). In examining the two somatic mutations found in intolerant residue R173 of RGS14, both R173C (Fig. 3, G and H) and R173H (Fig. 3, I and J) behaved as expected with both mutations exhibiting a LoF phenotype. In parallel, we assessed direct binding of each RGS14 mutation with active Gαo as measured by affinity capture by immunoprecipitation from HEK293 cell lysates treated with AlF_4^-/Mg^{++} (AMF) to activate cellular G proteins including of Gαo (Fig. 3K). We observed that the direct binding properties of the mutants mirrored that for RGS regulation of α2AR-Gαo activation. Specifically, mutant D137Y bound active Gαo, whereas mutants S127P, R173H and R173P all failed to bind Gαo (Fig. 3K). In summary, three of the four somatic mutations

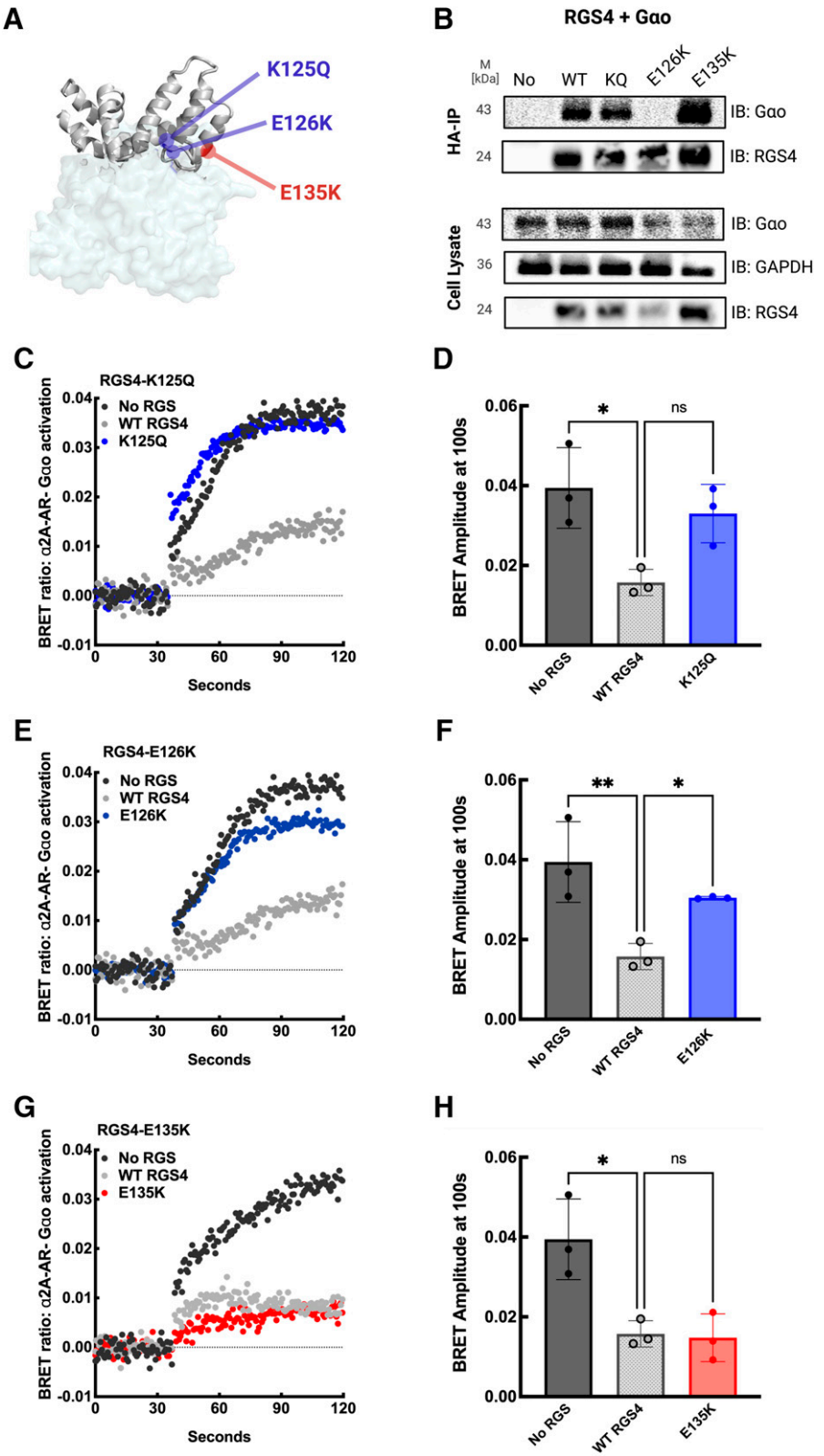

Fig. 5. Assessment of functional impact of RGS4 somatic mutations on GPCR-G protein activation and G protein binding. (A) Structural view of selected mutated tolerant (red) and intolerant (blue) residues in RGS4. (B) Coimmunoprecipitation studies show that RGS4 WT, K125Q and E135K mutants bound Gαo-AlF4-. Average whole traces of BRET signal over time ($n = 3$) are shown comparing WT and 3DMTR identified tolerant and intolerant residues HA-K125Q (C), HA-E126K (E) and HA-E135K (F). BRET amplitude at 100s observed from data presented for HA-K125Q (D), HA-E126K (F) and HA-E135K (G) comparison. Intolerant mutants HA-K125Q (C–D), HA-E126K (E–F) led to loss of function phenotypes while tolerant HA-E135K (G–H) did not. Error bars represent mean ± S.D. Statistical analysis was performed using one-way ANOVA with Dunnett's test (***$P < 0.0005$, **$P < 0.005$, *$P < 0.05$).

found in tolerant and intolerant residues of RGS14 as defined by 3DMTR behaved as predicted.

RGS10 is also part of the R12 subfamily, however, it is one of the smallest proteins in the RGS family and shares only a single conserved RGS domain in common with RGS14 and RGS12. Next, we examined the effects of selected somatic mutations on RGS10 functions using the same assay systems as described above (Fig. 4). In the case of RGS10, two somatic mutations were tested which were scored by 3DMTR as either tolerant (S64T) (Fig. 4, C and D) or intolerant (K89M) (Fig. 4, E and F). Wild-type RGS10 and mutant proteins expressed well in HEK293 cells (Supplemental Fig. 4B). The relative position of these residues within the RGS domain structure are shown in Fig. 4A highlighted as either red (tolerant) and blue (intolerant). Somatic mutations within the tolerant/intolerant residues of RGS10 exhibited phenotypes inconsistent with the 3DMTR prediction. Substituting a Thr for tolerant residue Ser64 (S64T) resulted in a partial LoF shown as a reduction in some, but not all capacity to inhibit receptor activation of G protein (Fig. 4, C and D). In contrast, substituting a Met for Lys (K89M) had no effect on RGS10 capacity to inhibit α2AR activation of Gαo (Fig. 4, E and F). Examining these results more closely, we find that residue K89 is located on an alpha helix away from the Gα binding interface, while S64 is located within the binding interface (Fig. 4A). This could explain why mutations at these sites resulted in the observed phenotype, though opposite of what would be expected from the 3DMTR prediction. However, we cannot rule of the possibility that substitution mutations to intolerant residue K89 may lead to other change of function (CoF).

We also measured direct RGS10 binding to active Gαo (Fig. 4B). Results showed that the mutant phenotypes matched the functional readouts for RGS10 regulation of receptor G activation. That is, mutant K89M bound active Gαo whereas mutant S64T did not. The fact that S64T showed some capacity to inhibit receptor-G activation but did not bind Gαo in the pulldown assay may reflect reduced affinity of this mutation for binding Gα. In summary, neither of the two somatic mutations found in tolerant and intolerant residues of RGS10 as defined by 3DMTR behaved as predicted in this assay.

RGS4 belongs to the B/R4 subfamily of RGS proteins, it is a small structure composed of only the RGS domain and has been linked to many cancers by regulating cell proliferation and apoptosis (Park et al., 2017; Xue et al., 2017; He et al., 2019). It has also been associated with enhanced glioma cell motility, thyroid carcinoma, and ovarian cancer (Tatenhorst et al., 2004; Nikolova et al., 2008; Hurst and Hooks, 2009; Hurst et al., 2009). RGS4 has been linked to reduced protein expression in metastatic tumors in breast cancer migration (Xie et al., 2009), suggesting that RGS4 enhancement can potentially block invasion (Sjogren 2011). The relative position of selected somatic mutations on RGS4 are shown in Fig. 5A highlighted as either red (tolerant) and blue (intolerant). As with RGS14 and RGS10, we measured the effects of RGS4 on α2AR-directed Gαo activation and direct RGS binding to Gαo in cell lysates. For RGS4, three somatic mutations were tested which were scored by 3DMTR as either intolerant (K125Q and E126K) (Fig. 5, C–F) or tolerant (E135K) (Fig. 5, G and H). Unlike RGS14 and RGS10, wild-type RGS4 failed to completely inhibit α2AR-directed Gαo activation, as we've reported before (Brown et al., 2016). RGS4 inhibited Gαo activation by approximately 75%. Intolerant mutants K125Q and E126K of RGS4 each exhibit partial loss-of-function phenotypes (Fig. 5, C–F), largely failing to inhibit Gαo activation, whereas tolerant mutation E135K (Fig. 5, G and H) behaved as wild-type RGS4.

We next examined the effects of somatic mutations on RGS4 capacity to bind directly to Gαo (Fig. 5B). Mutants K125Q and E135K each bound active Gαo, whereas mutant E126K did not bind. Intolerant mutant K125Q unexpectedly bound Gαo. It should be noted that the LoF effects observed for K125Q mutation (Fig. 5D) are only partial, and that the protein may be able to bind without fully exerting GAP effects on Gαo. RGS4 mutant E126K protein levels may be low in the cells (Supplemental Fig. 4C) but sufficiently high enough to exert GAP effects of Gαo.

The Impact of Somatic Mutations on RGS Protein Regulation of Intracellular cAMP Levels. Findings to this point examined the impact of cancer somatic mutations on RGS protein regulation of receptor-directed G protein activation and G protein binding. The second messenger cAMP (3′-5′-cyclic adenosine monophosphate) is ubiquitously expressed and regulates cell proliferation and differentiation via PKA/Epac1 activation (Vitale et al., 2009). The cAMP-PKA signaling pathway has been linked to play roles in tumor biology. For example, in glioblastoma, increasing levels of cAMP inhibit cell growth by upregulating p21/p27 and PKA/Epac1-Rap1 signaling (Chen et al., 1998, 2002; Moon et al., 2012; Zhang et al., 2020). We next tested the effects of the cancer somatic mutations in key residues of RGS proteins downstream of G protein activation. For this, we examined the functions of cancer mutations of either a tolerant or an intolerant residue for each RGS protein (R173C and D137Y for RGS14, S64T and K89M for RGS10, and E126K and E135K for RGS4) in Gαi/o-inhibition of adenylyl cyclase stimulated cAMP accumulation (Fig. 6). The accumulation of cAMP in live cells was measured using the luciferase-based GloSensor assay (Fig. 6A). Studies have shown RGS4 to regulate receptor and G protein–directed inhibition of AC (Huang et al., 1997), and RGS4 and RGS10 to inhibit forskolin stimulated cAMP production in CHOK1 cells stably expressing 5-HT1A receptor (Ghavami et al., 2004). However, the effect of RGS14, RGS10 and RGS4 effect on cAMP levels in cells expressing α2AR has not been explored. To measure RGS effects on receptor-Gαi/o inhibition of cellular cAMP, cells were stimulated first with α2AR-Gαi/o coupled agonist (100 μM UK 14,304) or vehicle (DMSO), followed by forskolin (10 μM FSK) to stimulate adenylyl cyclase (AC) production of cAMP (Fig. 6B). Of note, α2AR has been shown to couple to both Gs and Gαi/o in HEK cells (Wade et al., 1999). However, under the chosen experimental conditions, α2-AR-Gi/o coupling appears to dominate. That is, agonist activation of α2AR-Gαi/o significantly inhibited FSK-stimulated cAMP accumulation when compared with vehicle (Fig. 6C), indicating that FSK activation overrides any Gαs contribution to cAMP formation. In each case, wild-type RGS14, RGS10 and RGS4 reversed agonist-receptor-G protein inhibition of cAMP formation (Fig. 6, D–F), with RGS14 being more effective than RGS10 and RGS4. Intolerant mutant R173C in RGS14 lost capacity to reverse G protein inhibition of cAMP, whereas tolerant mutant D137Y showed a robust capacity to enhance cAMP

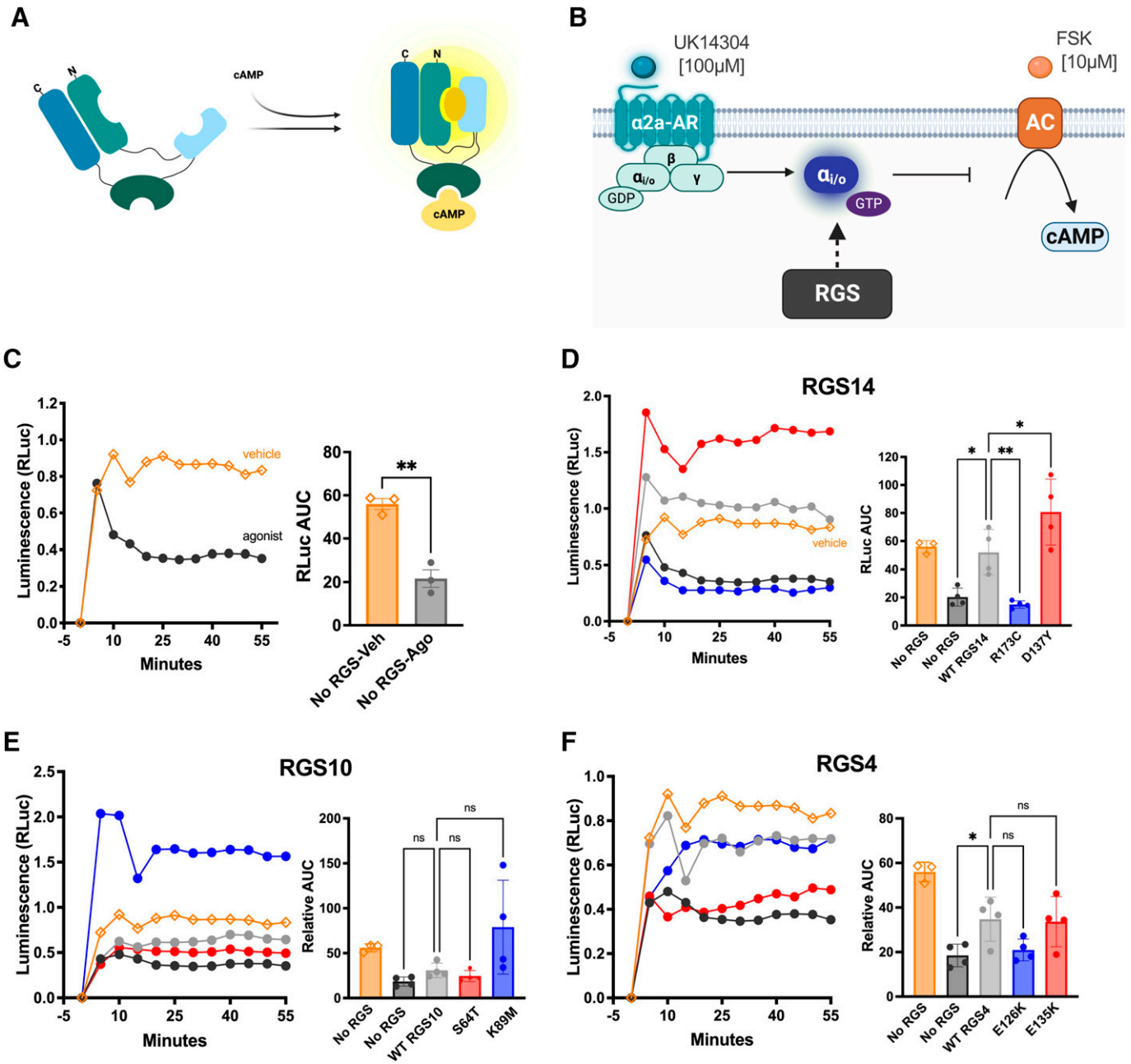

Fig. 6. Assessment of functional impact of wild-type versus mutant forms of RGS14, RGS10 and RGS4 on α2A-AR-G protein directed inhibition of cAMP levels. HEK293 cells were transfected with constructs encoding GloSensor cAMP reporter, α2A-AR, and RGS proteins of interest. At time 0, cells were treated with vehicle (DMSO) or agonist (● 100 μM of UK 14,304). After a 10-minute incubation at RT, cells were stimulated with FSK (10 μM). Luminescence intensity indicative of cAMP production was measured every 5 minutes for up to 50 minutes at room temperature. Values shown in each time-course panel are means of triplicates from individual experiments, representative of three to four independent experiments. Data shown as ±S.D.; $n = 3$ to 4 independent experiments represent the relative luminescence intensity AUC (Area under the curve). (A) Schematic representation of the GloSensor cAMP reporter and (B) schematic representation of the assay design. (C) In the absence of RGS proteins, FSK alone increases cAMP levels while agonist-Gai/o stimulation leads to a significant decrease in cAMP. Bar graph shows comparative data values of AUC. (D) RGS14 WT compared with mutants resulted in significantly different cAMP levels over time. Bar graph shows comparative data values of AUC. (E) Comparison between RGS10 and mutants did not lead to any significant differences. Bar graph shows comparative data values of AUC. (F) Comparison between RGS4 and mutants did not lead to any significant differences. Bar graph shows comparative data values of AUC. Statistical analysis was performed measuring the AUC, using unpaired t test for C, and one-way ANOVA and Dunnett's multiple comparison test for D–F (*$P < 0.05$, **$P < 0.005$).

accumulation (Fig. 6D). Interestingly, tolerant mutation S64T in RGS10 acted like WT RGS10, opposite to the effects in receptor-directed G protein activation and G protein binding (Fig. 4, B–D), while intolerant mutant K89M showed a robust capacity to enhance cAMP accumulation (Fig. 6E). Intolerant mutant E126K in RGS4 lost the capacity to reverse G protein inhibition of cAMP, while tolerant mutant E135K acted like RGS4 WT (Fig. 6F). The same trends were observed here as was for receptor-directed G protein activation and G protein binding (Fig. 5, B and E–H).

Several studies have identified RGS proteins to be regulators of adenylyl cyclase (AC) activity. RGS2 decreases accumulation

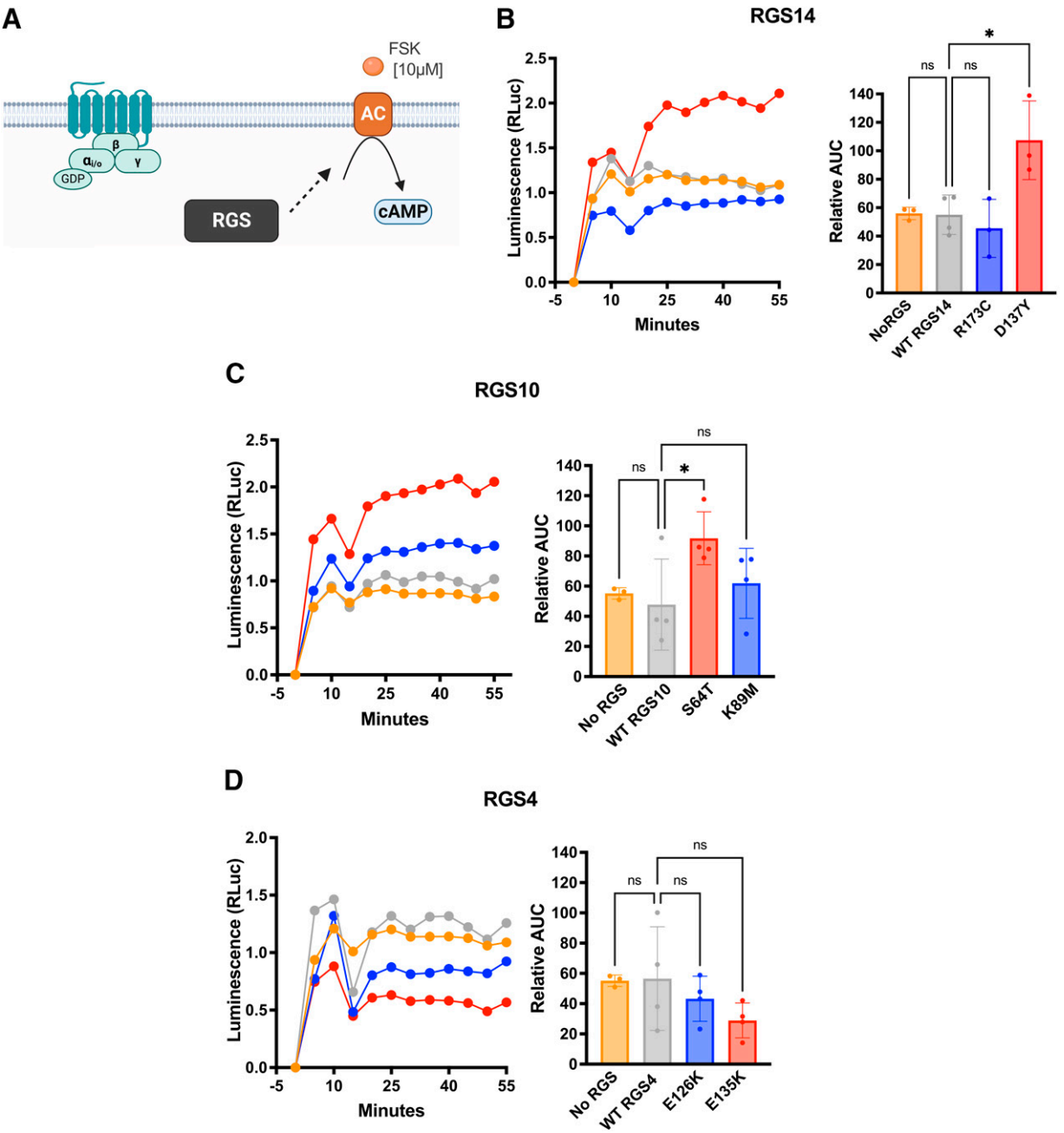

Fig. 7. Assessment of the functional impact of wild-type versus mutant forms of RGS14, RGS10 and RGS4 on FSK-stimulated cAMP production by adenylyl cyclase (AC). HEK293 cells were transfected with constructs encoding GloSensor cAMP reporter, α2A-AR, and RGS proteins of interest. At time 0, cells were treated with vehicle (DMSO) and after a 10-minute incubation at RT, cells were stimulated with FSK (10 μM). Luminescence intensity indicative of cAMP production was measured every 5 minutes for 50 minutes at room temperature. Values shown in each time-course panel are means of triplicates from individual experiments, representative of three to four independent experiments. Data shown as ±S.D.; $n = 3$ to 4 independent experiments represent the relative luminescence intensity AUC. (A) Schematic representation of the assay measuring the effects of RGS proteins in AC stimulated cAMP. (B) RGS14-D137Y led to a significant increase in AC stimulated cAMP levels compared with WT and other mutants. Bar graph shows comparative data values of AUC. (C) RGS10-S64T led to a significant increase in AC stimulated cAMP levels compared with WT and other mutants. Bar graph shows comparative data values of AUC. (D) There was no significant difference between RGS4 WT and mutants. Bar graph shows comparative data values of AUC. Statistical analysis was performed measuring the AUC and analyzing the difference between the conditions using one-way ANOVA and Dunnett's multiple comparison test (*$P < 0.05$).

of cAMP by directly interacting with type V AC (Salim et al., 2003; Roy et al., 2006), and RGS4 and RGS10 inhibited G protein–independent cAMP production in CHOK1 cells (Ghavami et al., 2004). However, the actions of RGS14 on AC activity has not been explored. Therefore, we next examined the effect of RGS proteins on forskolin-stimulated cAMP production directly, in the absence of agonist-activated α2AR-G protein contributions (Fig. 7A). Results for WT RGS14, RGS10 and RGS4 (Fig. 7, B–D) did not show an inhibition of FSK-stimulated cAMP levels in HEK293 cells transfected with α2-AR without agonist stimulation. Tolerant mutant D137Y in

TABLE 2
The 3DMTR analysis is a better predictor of key protein residues for functional impact of somatic mutations than 1DMTR
Summary results of the multiple functional assessments performed to characterize the effects of the reported mutations. Overall, the 3DMTR analysis is a better predictor of intolerant protein regions than 1DMTR. With this information we can better predict which reported mutations will lead to a change-of-function phenotype.

RGS	Selected Mutation	1DMTR Score	CoF Prediction	3DMTR Score	CoF Prediction	CoF Effect	Matched 3DMTR
RGS14	S127P	1.04	No	1.03	No	GoF	x
	D137Y	1.08	No	0.93	No	GoF	●
	R173C	0.92	No	0.50	Yes	LoF	●
	R173H	0.92	No	0.50	Yes	LoF	●
RGS10	S64T	0.85	No	0.91	No	Mixed	x
	K89M	0.69	No	0.48	Yes	Mixed	x
RGS4	K125Q	0.94	No	0.48	Yes	LoF	●
	E126K	0.99	No	0.42	Yes	LoF	●
	E135K	1.22	No	1.14	No	WT	●

●, matched prediction; x, no match.

RGS14 showed a robust increase in cAMP levels in the absence of agonist-stimulated Gi/o-coupled receptor (Fig. 7B). Interestingly, tolerant mutant S64T in RGS10 showed an increase in cAMP levels when compared with WT RGS10 that had no effect (Fig. 7C). This trend is the opposite of the results shown in the previous assay of RGS10 mutant effects on receptor inhibition of cAMP (Fig. 6E). Mutations in E126K and E135K of RGS4 showed similar results to the effects shown for WT RGS4 (Fig. 6F).

Discussion

3DMTR Analysis Is a More Accurate Predictor Than 1DMTR. In the present study, we performed a functional assessment of the predictive capabilities of the novel 3DMTR analysis applied to RGS proteins. The MTR method analyzes the regional intolerance to mutations in proteins of interest (Traynelis et al., 2017). Recent efforts have refined this tool and improved its predictive qualities (Perszyk et al., 2021). Using the 3D protein structure allows for a more refined and accurate prediction of important protein regions as it is common for non-adjacent segments of the polypeptide chain to come together in the tertiary and quaternary structure of a protein. We were able to identify important residues that show intolerance to genetic variance in most RGS domains of the RGS analogs that had a reported protein structure (Supplemental Figs. 1 and 2). Our results show that the 3DMTR analysis is a more accurate predictor of regional intolerance when compared with its 1DMTR (Table 2). When we compared against the predictive qualities of other bioinformatic tools (SIFT, PROVEAN, MutPRED2; Supplemental Tables 2–4), 3DMTR was the most accurate at predicting intolerant residues of the protein that, if mutated, would lead to deleterious effects and change-of-function phenotypes. All nine selected residues in RGS14, RGS10 and RSG4 were predicted to be tolerant to change by the 1DMTR, while the 3DMTR predicted five of nine to be intolerant to change. The 3DMTR identified intolerant and tolerant mutated residues affected in GPCR-G protein activation and G protein binding. For RGS14, three of four, and three of three for RGS4 matched the 3DMTR-permutaiton analysis predictions. RGS10 mutants gave results that were opposite of expected in GPCR-G protein activation and G protein binding assessments.

While greatly improved over the 1DMTR, the 3DMTR analysis was not perfect in it is predictive power, with discrepancies noted after some functional assessments. The function of an RGS protein in GPCR-G protein activation and G protein binding is dependent on residue selectivity (Xie and Palmer, 2007). When the mutations examined here were tested downstream of the GPCR for RGS14 and RGS4 (e.g., cAMP accumulation), the intolerant and tolerant mutants behaved as expected in most, but not all cases. For example, the tolerant residue D137Y in RGS14 presented as tolerant in the Gα coupling assay, but showed an unexpected enhanced gain-of-function effect in the cAMP assay. Another example of a mutant with a conflicting phenotype was intolerant residue K89M in RGS10. We found that K89M was tolerant and behaved as wild-type protein in the G protein coupling assay but exhibited altered function in the assessment of inhibition of Gi/o-inhibition of cAMP levels causing an enhanced activity. In both cases, the cAMP assay measures adenylyl cyclase (AC) activity, and it should be noted that some RGS proteins bind directly to certain AC isoforms to stimulate their activity (Salim et al., 2003; Roy et al., 2006). In this case, tolerant D137Y RGS14 mutant and intolerant K89M RGS10 mutants could interact directly with AC, or the AC-Gα complex, to stimulate AC enzyme activity. Consistent with this idea, our findings in Fig. 7 indicate enhanced AC activity with these mutants in the absence of receptor agonist. Alternatively, the functional assessment of these assays relies on the network of residues that make direct contact with the active Gα. The intolerant K89M mutation is found away from the binding site in RGS10, and this could explain why it did not lead to an altered loss-of-function phenotype in G protein coupling but did exhibit a phenotype in the cAMP assay. As a tangential side note, RGS actions on AC have not been extensively studied. Our observations of RGS mutant effects on forskolin-stimulated AC raises the question of whether RGS proteins in general regulate AC differently with forskolin versus GPCR-Gs-activation, a topic for future study.

Despite these examples, the 3DMTR was a good overall predictor of intolerant residues that resulted in a change-of-function. The 3DMTR results need to be placed in perspective compared with other available tools, that are demonstrably less accurate predictors of change-of-function. For example, and as noted above, the COSMIC-FATHMM-MKL algorithm inexplicably designated silent mutations in residues N93, A99 and R173 of RGS14 to be pathogenic which, of course, is not possible at the protein level. In the future, the 3DMTR may also develop into a more precise tool. Specifically, as the Genome Aggregation Database (gnomAD) source data for the method collects more human synonymous and missense variant information, the analysis may be more accurate and/or require fewer residues to aggregate data that may lead to improved predictive potential.

RGS Proteins in Cancer and the Impact of Linked Mutations in Signaling Pathways. Roles for RGS proteins in GPCR-G protein signaling in human cancer have not been extensively studied, though genetic variants in RGS proteins linked to cancer have been reported (Dai et al., 2011; Lee et al., 2013; Qutob et al., 2018; DiGiacomo et al., 2020). GPCRs have been shown to play a role in the initiation and progression of cancer, suggesting that regulators of GPCRs are also important in regulating oncogenic pathways. However, the specific roles of RGS proteins in regulating oncogenic pathways are still being studied.

In this study, we examined cancer associated mutations in RGS proteins that overlap with the significant residues identified by 3DMTR analysis. Of note, most cancer-linked mutations in RGS proteins have not been tested, except for a recent report (DiGiacomo et al., 2020). Here we tested nine cancer-linked mutations across three different RGS proteins for their functional phenotypes. These nine mutants were tested because they overlapped with residues predicted by 3DMTR to be either tolerant or intolerant to change and were predicted by the FATHMM analysis to have deleterious effect in protein function. These cancer-linked mutations were tested for their capacity to impact GPCR-G protein signaling. GPCR signaling can be altered by aberrant receptor overexpression, gain-of-function activating receptor, or mutations in downstream G protein signaling effectors, like RGS proteins, that favor oncogenicity (Gutkind, 1998). A recent study has identified 475 mutations reported in the RGS domain of RGS proteins present in 22 cancer types (DiGiacomo et al., 2020). We explored the functional effects that cancer associated mutants have in regulating RGS-G protein activation and downstream effector signaling. Eight out of the nine tested mutants led to a change-of-function phenotype. Tightly regulated GPCR-G protein-RGS signaling pathways control many important physiologic events. GPCRs show selectivity to Gα-subtypes as well as RGS proteins (Xie and Palmer, 2007) and activate/regulate specific downstream second messenger signaling pathways (e.g., cAMP) to mediate cell migration and survival (O'Hayre et al., 2014). Mutations in RGS proteins can lead to GPCR signaling dysregulation, which has been linked to roles in certain cancers (Arang and Gutkind, 2020; DiGiacomo et al., 2020). Loss-of-function mutations in RGS proteins, like RGS14-R173C/H and RGS4-E126K/K125Q, could increase G protein activity serving to promote tumor growth mechanisms (Nishihara et al., 2004). Likewise, RGS genetic variations also could be associated with patient response to chemotherapies that specifically target GPCRs (Dai et al., 2011).

Recent advances in genome technology have allowed for a better understanding of the contribution of intolerant genetic variants in cancer pathogenesis. This, in turn, has allowed for improved diagnosis, and improved selection of cancer treatments in personalized medicine. Tools such as the novel 3DMTR analysis could enable biomedical researchers to prioritize which mutations/residues should be tested first for studying change-of-function phenotypes. Examples of this approach in other disease states such as idiopathic epilepsy have yielded remarkably promising results (EpiPM, 2015; Perszyk et al., 2021). Because bioinformatic tools are not perfect, the major challenge will be to make biologic sense of data from large publicly available disease-linked genetic data bases and computational analysis. Our small-scale project is an example of how using the correct bioinformatic tools and testing that tool's predictive capabilities can elucidate the role of understudied genetic variants in RGS and other proteins in cancer disease progression.

Acknowledgments

We thank Miss Juleva Doan and Dr. Randy Hall for the assistance with the cAMP GloSensor assay, and Dr. Nevin Lambert for the generous gift of the BRET biosensors.

Authorship Contributions

Participated in research design: Montañez-Miranda, Perszyk, Traynelis, Hepler.

Conducted experiments: Montañez-Miranda, Harbin, Okalova, Ramineni.

Performed data analysis: Montañez-Miranda, Perszyk.

Wrote or contributed to the writing of the manuscript: Montañez-Miranda, Perszyk, Harbin, Hepler.

References

Ali MW, Cacan E, Liu Y, Pierce JY, Creasman WT, Murph MM, Govindarajan R, Eblen ST, Greer SF, and Hooks SB (2013) Transcriptional suppression, DNA methylation, and histone deacetylation of the regulator of G-protein signaling 10 (RGS10) gene in ovarian cancer cells. *PLoS One* **8**:e60185.

Alqinyah M, Almutairi F, Wendimu MY, and Hooks SB (2018) RGS10 regulates the expression of cyclooxygenase-2 and tumor necrosis factor alpha through a G protein-independent mechanism. *Mol Pharmacol* **94**:1103–1113.

Arang N and Gutkind JS (2020) G protein-coupled receptors and heterotrimeric G proteins as cancer drivers. *FEBS Lett* **594**:4201–4232.

Bernstein LS, Ramineni S, Hague C, Cladman W, Chidiac P, Levey AI, and Hepler JR (2004) RGS2 binds directly and selectively to the M1 muscarinic acetylcholine receptor third intracellular loop to modulate Gq/11alpha signaling. *J Biol Chem* **279**:21248–21256.

Brown NE, Lambert NA, and Hepler JR (2016) RGS14 regulates the lifetime of Gα-GTP signaling but does not prolong Gβγ signaling following receptor activation in live cells. *Pharmacol Res Perspect* **4**:e00249.

Cacan E, Ali MW, Boyd NH, Hooks SB, and Greer SF (2014) Inhibition of HDAC1 and DNMT1 modulate RGS10 expression and decrease ovarian cancer chemoresistance. *PLoS One* **9**:e87455.

Chaudhary PK and Kim S (2021) An insight into GPCR and G-proteins as cancer drivers. *Cells* **10**:3288.

Chen TC, Hinton DR, Zidovetzki R, and Hofman FM (1998) Up-regulation of the cAMP/PKA pathway inhibits proliferation, induces differentiation, and leads to apoptosis in malignant gliomas. *Lab Invest* **78**:165–174.

Chen TC, Wadsten P, Su S, Rawlinson N, Hofman FM, Hill CK, and Schönthal AH (2002) The type IV phosphodiesterase inhibitor rolipram induces expression of the cell cycle inhibitors p21(Cip1) and p27(Kip1), resulting in growth inhibition, increased differentiation, and subsequent apoptosis of malignant A-172 glioma cells. *Cancer Biol Ther* **1**:268–276.

Cho H, Kozasa T, Takekoshi K, De Gunzburg J, and Kehrl JH (2000) RGS14, a GTPase-activating protein for Gialpha, attenuates Gialpha- and G13alpha-mediated signaling pathways. *Mol Pharmacol* **58**:569–576.

Dai J, Gu J, Lu C, Lin J, Stewart D, Chang D, Roth JA, and Wu X (2011) Genetic variations in the regulator of G-protein signaling genes are associated with survival in late-stage non-small cell lung cancer. *PLoS One* **6**:e21120.

DiGiacomo V, Maziarz M, Luebbers A, Norris JM, Laksono P, and Garcia-Marcos M (2020) Probing the mutational landscape of regulators of G protein signaling proteins in cancer. *Sci Signal* **13**:eaax8620.

Dou Y, Gold HD, Luquette LJ, and Park PJ (2018) Detecting somatic mutations in normal cells. *Trends Genet* **34**:545–557.

EpiPM Consortium (2015) A roadmap for precision medicine in the epilepsies. *Lancet Neurol* **14**:1219–1228.

Friedman PA, Sneddon WB, Mamonova T, Montanez-Miranda C, Ramineni S, Harbin NH, Squires KE, Gefter JV, Magyar CE, Emlet DR, et al. (2022) RGS14 regulates PTH- and FGF23-sensitive NPT2A-mediated renal phosphate uptake via binding to the NHERF1 scaffolding protein. *J Biol Chem* **298**:101836.

Garcia-Marcos M, Ghosh P, and Farquhar MG (2011) Molecular basis of a novel oncogenic mutation in GNAO1. *Oncogene* **30**:2691–2696.

Ghavami A, Hunt RA, Olsen MA, Zhang J, Smith DL, Kalgaonkar S, Rahman Z, and Young KH (2004) Differential effects of regulator of G protein signaling (RGS) proteins on serotonin 5-HT1A, 5-HT2A, and dopamine D2 receptor-mediated signaling and adenylyl cyclase activity. *Cell Signal* **16**:711–721.

Goldenstein BL, Nelson BW, Xu K, Luger EJ, Pribula JA, Wald JM, O'Shea LA, Weinshenker D, Charbeneau RA, Huang X, et al. (2009) Regulator of G protein signaling protein suppression of Galphao protein-mediated alpha2A adrenergic receptor inhibition of mouse hippocampal CA3 epileptiform activity. *Mol Pharmacol* **75**:1222–1230.

Gutkind JS (1998) Cell growth control by G protein-coupled receptors: from signal transduction to signal integration. *Oncogene* **17** (11 Reviews):1331–1342.

Harbin NH, Bramlett SN, Montanez-Miranda C, Terzioglu G, and Hepler JR (2021) RGS14 regulation of post-synaptic signaling and spine plasticity in brain. *Int J Mol Sci* **22**:6823.

He Z, Yu L, Luo S, Li Q, Huang S, and An Y (2019) RGS4 regulates proliferation and apoptosis of NSCLC cells via microRNA-16 and brain-derived neurotrophic factor. *OncoTargets Ther* **12**:8701–8714.
Hepler JR (1999) Emerging roles for RGS proteins in cell signalling. *Trends Pharmacol Sci* **20**:376–382.
Hepler JR, Berman DM, Gilman AG, and Kozasa T (1997) RGS4 and GAIP are GTPase-activating proteins for Gq alpha and block activation of phospholipase C beta by gamma-thio-GTP-Gq alpha. *Proc Natl Acad Sci USA* **94**:428–432.
Hollinger S and Hepler JR (2002) Cellular regulation of RGS proteins: modulators and integrators of G protein signaling. *Pharmacol Rev* **54**:527–559.
Hollinger S, Taylor JB, Goldman EH, and Hepler JR (2001) RGS14 is a bifunctional regulator of Galphai/o activity that exists in multiple populations in brain. *J Neurochem* **79**:941–949.
Hollins B, Kuravi S, Digby GJ, and Lambert NA (2009) The c-terminus of GRK3 indicates rapid dissociation of G protein heterotrimers. *Cell Signal* **21**:1015–1021.
Hooks SB, Callihan P, Altman MK, Hurst JH, Ali MW, and Murph MM (2010) Regulators of g-protein signaling RGS10 and RGS17 regulate chemoresistance in ovarian cancer cells. *Mol Cancer* **9**:289.
Huang C, Hepler JR, Gilman AG, and Mumby SM (1997) Attenuation of Gi- and Gq-mediated signaling by expression of RGS4 or GAIP in mammalian cells. *Proc Natl Acad Sci USA* **94**:6159–6163.
Hunt TW, Fields TA, Casey PJ, and Peralta EG (1996) RGS10 is a selective activator of G alpha i GTPase activity. *Nature* **383**:175–177.
Hurst JH and Hooks SB (2009) Regulator of G-protein signaling (RGS) proteins in cancer biology. *Biochem Pharmacol* **78**:1289–1297.
Hurst JH, Mendpara N, and Hooks SB (2009) Regulator of G-protein signalling expression and function in ovarian cancer cell lines. *Cell Mol Biol Lett* **14**:153–174.
Ideno N, Yamaguchi H, Ghosh B, Gupta S, Okumura T, Steffen DJ, Fisher CG, Wood LD, Singhi AD, Nakamura M, et al. (2018) $GNAS^{R201C}$ induces pancreatic cystic neoplasms in mice that express activated KRAS by inhibiting YAP1 signaling. *Gastroenterology* **155**:1593–1607.e12.
Kan Z, Jaiswal BS, Stinson J, Janakiraman V, Bhatt D, Stern HM, Yue P, Haverty PM, Bourgon R, Zheng J, et al. (2010) Diverse somatic mutation patterns and pathway alterations in human cancers. *Nature* **466**:869–873.
Lambert NA, Johnston CA, Cappell SD, Kuravi S, Kimple AJ, Willard FS, and Siderovski DP (2010) Regulators of G-protein signaling accelerate GPCR signaling kinetics and govern sensitivity solely by accelerating GTPase activity. *Proc Natl Acad Sci USA* **107**:7066–7071.
Lee EK, Ye Y, Kamat AM, and Wu X (2013) Genetic variations in regulator of G-protein signaling (RGS) confer risk of bladder cancer. *Cancer* **119**:1643–1651.
Masuho I, Balaji S, Muntean BS, Skamangas NK, Chavali S, Tesmer JJG, Babu MM, and Martemyanov KA (2020) A global map of G protein signaling regulation by RGS proteins. *Cell* **183**:503–521.e19.
McCoy KL and Hepler JR (2009) Regulators of G protein signaling proteins as central components of G protein-coupled receptor signaling complexes. *Prog Mol Biol Transl Sci* **86**:49–74.
Moon EY, Lee GH, Lee MS, Kim HM, and Lee JW (2012) Phosphodiesterase inhibitors control A172 human glioblastoma cell death through cAMP-mediated activation of protein kinase A and Epac1/Rap1 pathways. *Life Sci* **90**:373–380.
Moore AR, Ceraudo E, Sher JJ, Guan Y, Shoushtari AN, Chang MT, Zhang JQ, Walczak EG, Kazmi MA, Taylor BS, et al. (2016) Recurrent activating mutations of G-protein-coupled receptor CYSLTR2 in uveal melanoma. *Nat Genet* **48**:675–680.
Nairismägi ML, Tan J, Lim JQ, Nagarajan S, Ng CC, Rajasegaran V, Huang D, Lim WK, Laurensia Y, Wijaya GC, et al. (2016) JAK-STAT and G-protein-coupled receptor signaling pathways are frequently altered in epitheliotropic intestinal T-cell lymphoma. *Leukemia* **30**:1311–1319.
Nikolova DN, Zembutsu H, Sechanov T, Vidinov K, Kee LS, Ivanova R, Becheva E, Kocova M, Toncheva D, and Nakamura Y (2008) Genome-wide gene expression profiles of thyroid carcinoma: identification of molecular targets for treatment of thyroid carcinoma. *Oncol Rep* **20**:105–121.
Nishihara H, Hwang M, Kizaka-Kondoh S, Eckmann L, and Insel PA (2004) Cyclic AMP promotes cAMP-responsive element-binding protein-dependent induction of cellular inhibitor of apoptosis protein-2 and suppresses apoptosis of colon cancer cells through ERK1/2 and p38 MAPK. *J Biol Chem* **279**:26176–26183.
Nobles M, Benians A, and Tinker A (2005) Heterotrimeric G proteins precouple with G protein-coupled receptors in living cells. *Proc Natl Acad Sci USA* **102**:18706–18711.
Nobrega MA and Pennacchio LA (2004) Comparative genomic analysis as a tool for biological discovery. *J Physiol* **554**:31–39.
O'Hayre M, Vázquez-Prado J, Kufareva I, Stawiski EW, Handel TM, Seshagiri S, and Gutkind JS (2013) The emerging mutational landscape of G proteins and G-protein-coupled receptors in cancer. *Nat Rev Cancer* **13**:412–424.
O'Hayre M, Degese MS, and Gutkind JS (2014) Novel insights into G protein and G protein-coupled receptor signaling in cancer. *Curr Opin Cell Biol* **27**:126–135.
Olafsson S and Anderson CA (2021) Somatic mutations provide important and unique insights into the biology of complex diseases. *Trends Genet* **37**:872–881.
Park HJ, Kim SH, and Moon DO (2017) Growth inhibition of human breast carcinoma cells by overexpression of regulator of G-protein signaling 4. *Oncol Lett* **13**:4357–4363.
Perszyk RE, Kristensen AS, Lyuboslavsky P, and Traynelis SF (2021) Three-dimensional missense tolerance ratio analysis. *Genome Res* **31**:1447–1461.
Popov S, Yu K, Kozasa T, and Wilkie TM (1997) The regulators of G protein signaling (RGS) domains of RGS4, RGS10, and GAIP retain GTPase activating protein activity in vitro. *Proc Natl Acad Sci USA* **94**:7216–7220.
Puiffe ML, Le Page C, Filali-Mouhim A, Zietarska M, Ouellet V, Tonin PN, Chevrette M, Provencher DM, and Mes-Masson AM (2007) Characterization of ovarian cancer ascites on cell invasion, proliferation, spheroid formation, and gene expression in an in vitro model of epithelial ovarian cancer. *Neoplasia* **9**:820–829.
Qutob N, Masuho I, Alon M, Emmanuel R, Cohen I, Di Pizio A, Madore J, Elkahloun A, Ziv T, Levy R, et al. (2018) RGS7 is recurrently mutated in melanoma and promotes migration and invasion of human cancer cells. *Sci Rep* **8**:653.
Roy AA, Baragli A, Bernstein LS, Hepler JR, Hébert TE, and Chidiac P (2006) RGS2 interacts with Gs and adenylyl cyclase in living cells. *Cell Signal* **18**:336–348.
Sakloth F, Polizu C, Bertherat F, and Zachariou V (2020) Regulators of G protein signaling in analgesia and addiction. *Mol Pharmacol* **98**:739–750.
Salim S, Sinnarajah S, Kehrl JH, and Dessauer CW (2003) Identification of RGS2 and type V adenylyl cyclase interaction sites. *J Biol Chem* **278**:15842–15849.
Schwarz E (2018) A gene-based review of RGS4 as a putative risk gene for psychiatric illness. *Am J Med Genet B Neuropsychiatr Genet* **177**:267–273.
Shihab HA, Rogers MF, Gough J, Mort M, Cooper DN, Day INM, Gaunt TR, and Campbell C (2015) An integrative approach to predicting the functional effects of non-coding and coding sequence variation. *Bioinformatics* **31**:1536–1543.
Shu FJ, Ramineni S, Amyot W, and Hepler JR (2007) Selective interactions between Gi alpha1 and Gi alpha3 and the GoLoco/GPR domain of RGS14 influence its dynamic subcellular localization. *Cell Signal* **19**:163–176.
Sjögren B (2011) Regulator of G protein signaling proteins as drug targets: current state and future possibilities. *Adv Pharmacol* **62**:315–347.
Sjögren B and Neubig RR (2010) Thinking outside of the "RGS box": new approaches to therapeutic targeting of regulators of G protein signaling. *Mol Pharmacol* **78**:550–557.
Soundararajan M, Willard FS, Kimple AJ, Turnbull AP, Ball LJ, Schoch GA, Gileadi C, Fedorov OY, Dowler EF, Higman VA, et al. (2008) Structural diversity in the RGS domain and its interaction with heterotrimeric G protein alpha-subunits. *Proc Natl Acad Sci USA* **105**:6457–6462.
Squires KE, Gerber KJ, Tillman MC, Lustberg DJ, Montañez-Miranda C, Zhao M, Ramineni S, Scharer CD, Saha RN, Shu FJ, et al. (2021) Human genetic variants disrupt RGS14 nuclear shuttling and regulation of LTP in hippocampal neurons. *J Biol Chem* **296**:100024.
Stewart A and Fisher RA (2015) Introduction: G protein-coupled receptors and RGS proteins. *Prog Mol Biol Transl Sci* **133**:1–11.
Tate JG, Bamford S, Jubb HC, Sondka Z, Beare DM, Bindal N, Boutselakis H, Cole CG, Creatore C, Dawson E, et al. (2019) COSMIC: the Catalogue of Somatic Mutations in Cancer. *Nucleic Acids Res* **47** (D1):D941–D947.
Tatenhorst L, Senner V, Püttmann S, and Paulus W (2004) Regulators of G-protein signaling 3 and 4 (RGS3, RGS4) are associated with glioma cell motility. *J Neuropathol Exp Neurol* **63**:210–222.
Terzi D, Stergiou E, King SL, and Zachariou V (2009) Regulators of G protein signaling in neuropsychiatric disorders. *Prog Mol Biol Transl Sci* **86**:299–333.
Tesmer JJ, Berman DM, Gilman AG, and Sprang SR (1997) Structure of RGS4 bound to AlF4–activated G(i alpha1): stabilization of the transition state for GTP hydrolysis. *Cell* **89**:251–261.
Thusberg J and Vihinen M (2009) Pathogenic or not? And if so, then how? Studying the effects of missense mutations using bioinformatics methods. *Hum Mutat* **30**:703–714.
Traver S, Bidot C, Spassky N, Baltauss T, De Tand MF, Thomas JL, Zalc B, Janoueix-Lerosey I, and Gunzburg JD (2000) RGS14 is a novel Rap effector that preferentially regulates the GTPase activity of galphao. *Biochem J* **350**:19–29.
Traynelis J, Silk M, Wang Q, Berkovic SF, Liu L, Ascher DB, Balding DJ, and Petrovski S (2017) Optimizing genomic medicine in epilepsy through a gene-customized approach to missense variant interpretation. *Genome Res* **27**:1715–1729.
Uhlen M, Zhang C, Lee S, Sjöstedt E, Fagerberg L, Bidkhori G, Benfeitas R, Arif M, Liu Z, Edfors F, et al. (2017) A pathology atlas of the human cancer transcriptome. *Science* **357**:eaan2507.
Van Raamsdonk CD, Bezrookove V, Green G, Bauer J, Gaugler L, O'Brien JM, Simpson EM, Barsh GS, and Bastian BC (2009) Frequent somatic mutations of GNAQ in uveal melanoma and blue naevi. *Nature* **457**:599–602.
Van Raamsdonk CD, Griewank KG, Crosby MB, Garrido MC, Vemula S, Wiesner T, Obenauf AC, Wackernagel W, Green G, Bouvier N, et al. (2010) Mutations in GNA11 in uveal melanoma. *N Engl J Med* **363**:2191–2199.
Vellano CP, Brown NE, Blumer JB, and Hepler JR (2013) Assembly and function of the regulator of G protein signaling 14 (RGS14)·H-Ras signaling complex in live cells are regulated by Gαi1 and Gαi-linked G protein-coupled receptors. *J Biol Chem* **288**:3620–3631.
Vellano CP, Lee SE, Dudek SM, and Hepler JR (2011) RGS14 at the interface of hippocampal signaling and synaptic plasticity. *Trends Pharmacol Sci* **32**:666–674.
Vitale G, Dicitore A, Mari D, and Cavagnini F (2009) A new therapeutic strategy against cancer: cAMP elevating drugs and leptin. *Cancer Biol Ther* **8**:1191–1193.
Wade SM, Lim WK, Lan KL, Chung DA, Nanamori M, and Neubig RR (1999) G(i) activator region of alpha(2A)-adrenergic receptors: distinct basic residues mediate G(i) versus G(s) activation. *Mol Pharmacol* **56**:1005–1013.
Watson N, Linder ME, Druey KM, Kehrl JH, and Blumer KJ (1996) RGS family members: GTPase-activating proteins for heterotrimeric G-protein α-subunits. *Nature* **383**:172–175.
Weiler M, Pfenning PN, Thiepold AL, Blaes J, Jestaedt L, Gronych J, Dittmann LM, Berger B, Jugold M, Kosch M, et al. (2013) Suppression of proinvasive RGS4 by mTOR inhibition optimizes glioma treatment. *Oncogene* **32**:1099–1109.
Willars GB (2006) Mammalian RGS proteins: multifunctional regulators of cellular signalling. *Semin Cell Dev Biol* **17**:363–376.
Wright SC, Kozielewicz P, Kowalski-Jahn M, Petersen J, Bowin CF, Slodkowicz G, Marti-Solano M, Rodríguez D, Hot B, Okashah N, et al. (2019) A conserved molecular switch in class F receptors regulates receptor activation and pathway selection. *Nat Commun* **10**:667.
Wu J, Matthaei H, Maitra A, Dal Molin M, Wood LD, Eshleman JR, Goggins M, Canto MI, Schulick RD, Edil BH, et al. (2011) Recurrent GNAS mutations define an unexpected pathway for pancreatic cyst development. *Sci Transl Med* **3**:92ra66.
Xie GX and Palmer PP (2007) How regulators of G protein signaling achieve selective regulation. *J Mol Biol* **366**:349–365.
Xie Y, Wolff DW, Wei T, Wang B, Deng C, Kirui JK, Jiang H, Qin J, Abel PW, and Tu Y (2009) Breast cancer migration and invasion depend on proteasome degradation of regulator of G-protein signaling 4. *Cancer Res* **69**:5743–5751.

Xue X, Wang L, Meng X, Jiao J, and Dang N (2017) Regulator of G protein signaling 4 inhibits human melanoma cells proliferation and invasion through the PI3K/AKT signaling pathway. *Oncotarget* **8**: 78530–78544.

Yin W, Tang G, Zhou Q, Cao Y, Li H, Fu X, Wu Z, and Jiang X (2019) Expression profile analysis identifies a novel five-gene signature to improve prognosis prediction of glioblastoma. *Front Genet* **10**:419.

Zhang H, Kong Q, Wang J, Jiang Y, and Hua H (2020) Complex roles of cAMP-PKA-CREB signaling in cancer. *Exp Hematol Oncol* **9**:32.

Zhao P, Nunn C, Ramineni S, Hepler JR, and Chidiac P (2013) The Ras-binding domain region of RGS14 regulates its functional interactions with heterotrimeric G proteins. *J Cell Biochem* **114**:1414–1423.

Address correspondence to: Dr. John R. Hepler, Department of Pharmacology and Chemical Biology, Emory University School of Medicine, G205 O. Wayne Rollins Research Center, 1510 Clifton Road, Atlanta, GA 30320-3090. E-mail: Jhepler@emory.edu

Article title Functional assessment of cancer-linked mutations in sensitive regions of RGS proteins predicted by 3DMTR analysis

Authors : Carolina Montañez-Miranda, Riley E. Perszyk, Nicholas H. Harbin, Jennifer Okalova, Suneela Ramineni, Stephen F. Traynelis and John R. Hepler*

Primary lab of origin: Hepler lab, Department of Pharmacology and Chemical Biology, Emory University School of Medicine, Atlanta, Georgia 30322, USA (CMM, NHH, SR, JRH)

Journal Title: Molecular Pharmacology

Manuscript Number: MOLPHARM-AR-2022-000614

SUPPLEMENTARY INFORMATION

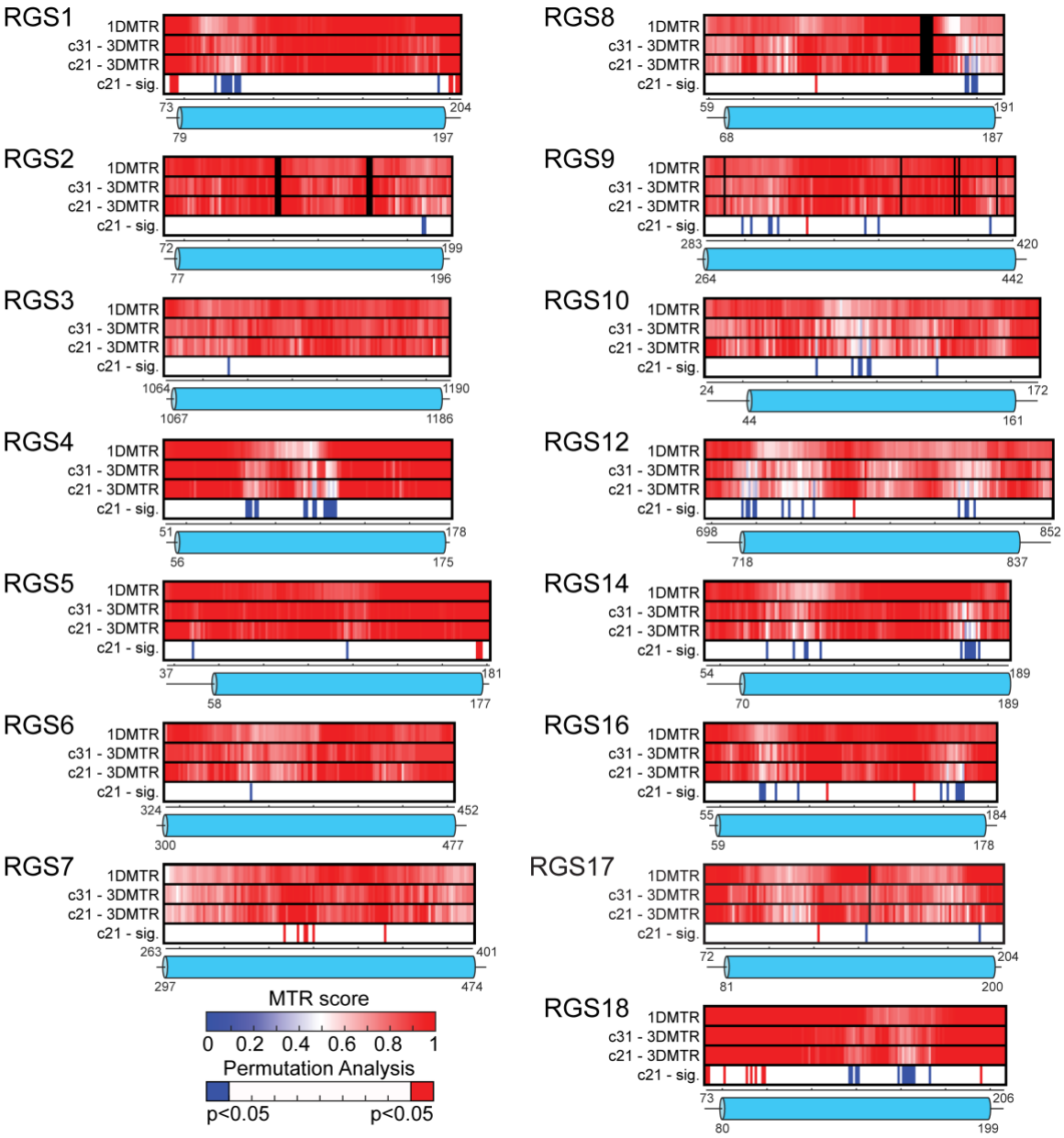

Supplemental Figure 1.Raster plot of all RGS proteins with available crystal structure.

The first row in each raster plot shows results from 1DMTR based on 31 neighboring residues in the liner sequence. Second row shows 3DMTR based on the 31 closest neighboring residues in 3D space. Third row shows 3DMTR based on the 21 closest neighboring residues. Fourth row shows significant residues based on the permutation analysis. Blue lines represent significantly (P<0.5) significant residues. Bottom blue cylinder represents the RGS domain of each protein with extreme N-terminal and C-terminal residues numbered.

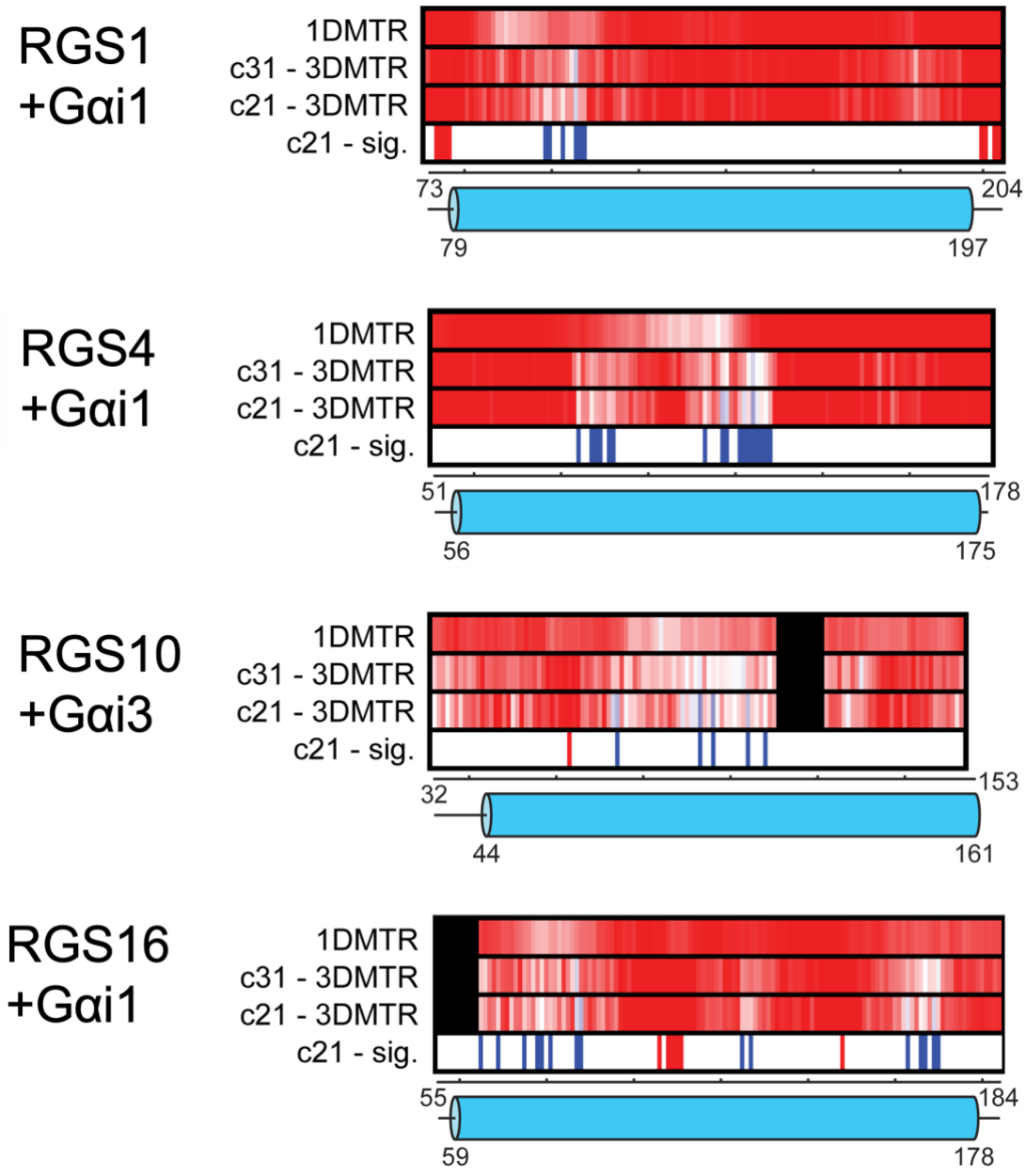

Supplemental Figure 2. Raster plot of RGS proteins in complex with active forms of their Gα partners. The MTR results were calculated using the RGS 3D structure that is found in complex with G alpha subunit**.** See Legend of Fig S1 for details. First row in the raster plot shows results from 1DMTR followed in the second row showing 3DMTR based on the 31 neighboring residues. Third row shows 3DMTR based on the 21 neighboring residues. Fourth row shows significant residues based on the permutation analysis (P<0.5). Bottom blue cylinder represents the RGS domain of each protein.

RGS protein	PDB	Deposition Authors	PMID	Link
RGS1	2BV1	Elkins, J.M., Yang, X., Soundararajan, M., et. al.	18434541	https://www.rcsb.org/structure/2BV1
RGS2	2AF0	Papagrigoriou, E., Johannson, C., Phillips, C., et. al.	18434541	https://www.rcsb.org/structure/2AF0
RGS3	2OJ4	Rezabkova, L., Boura, E., Herman, P., et. al.	20347994	https://www.rcsb.org/structure/2OJ4
RGS4	1AGR	Tesmer, J.J., Berman, D.M., Gilman, A.G., Sprang, S.R.	9108480	https://www.rcsb.org/structure/1AGR
RGS5	2CRP	Zhang, H.P., Hayashi, F., Yokoyama, S.	-	https://www.rcsb.org/structure/2CRP
RGS6	2ES0	Schoch, G.A., Phillips, C., Turnbull, A., et. al.	18434541	https://www.rcsb.org/structure/2ES0
RGS7	2D9J	Zhang, H.P., Nagasima, T., Hayashi, F., et. al.	-	https://www.rcsb.org/structure/2D9J
RGS8	2IHD	Turnbull, A.P., Papagrigoriou, E., Ugochukwu, E., et. al.	18434541	https://www.rcsb.org/structure/2ihd
RGS9	1FQI	Slep, K.C., Kercher, M.A., He, W., Cowan, C.W., Wensel, T.G., Sigler, P.B.	11234020	https://www.rcsb.org/structure/1FQI
RGS10	2DLR	Zhang, H.P., Nagashima, T., Hayashi, F., Yokoyama, S., RIKEN Structural Genomics/Proteomics Initiative (RSGI)	-	https://www.rcsb.org/structure/2DLR
RGS12	2EBZ	Zhang, H.P., Hayashi, F., Yokoyama, S., RIKEN Structural Genomics/Proteomics Initiative (RSGI)	-	https://www.rcsb.org/structure/2EBZ
RGS14	2JNU	Dowler, E.F., Diehl, A., Bray, J., et. al.	18434541	https://www.rcsb.org/structure/2JNU
RGS16	2BT2	Bunkoczi, G., Haroniti, A., Longman, E., et. al.	18434541	https://www.rcsb.org/structure/2BT2
RGS17	1ZV4	Schoch, G.A., Jansson, A., Elkins, J.M., et. al.	18434541	https://www.rcsb.org/structure/1ZV4
RGS18	2OWI	Higman, V.A., Leidert, M., Bray, J., et. al.	18434541	https://www.rcsb.org/structure/2OWI
RGS1 + Gαi1	2GTP	Soundararajan, M., Turnbull, A.P., Ugochukwu, E., et. al.	18434541	https://www.rcsb.org/structure/2GTP
RGS4 + Gαi1	1AGR	Tesmer, J.J., Berman, D.M., Gilman, A.G., Sprang, S.R.	9108480	https://www.rcsb.org/structure/1AGR
RGS10 + Gαi3	2IHB	Soundararajan, M., Turnbull, A.P., Papagrigoriou, E., et. al.	18434541	https://www.rcsb.org/structure/2IHB
RGS16 + Gαi1	2IK8	Soundararajan, M., Turnbull, A.P., Papagrigoriou, E., et. al.	18434541	https://www.rcsb.org/structure/2IK8

Supplemental Table 1. 3D structure information for analyzed RGS proteins. Protein Data Bank (PDB) information are shown for the 3D structures used in the analysis. In addition, the list of authors who submitted the structure, the PMID where the structure was cited, and the link to the pdb database are shown.

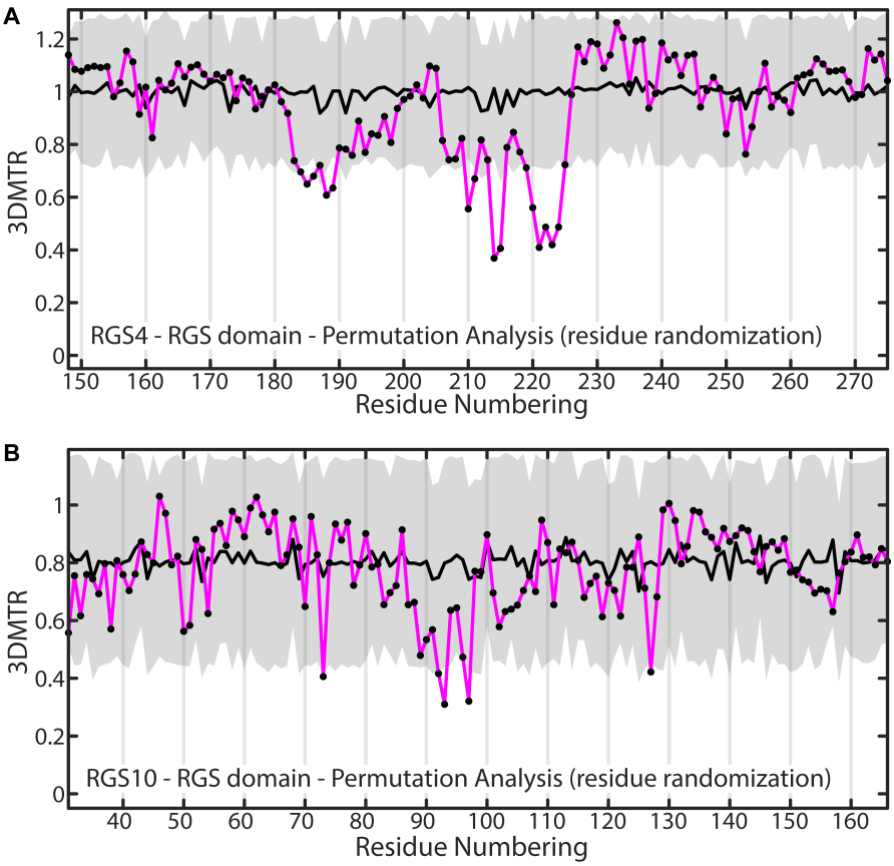

Supplemental Fig 3. 3DMTR-permutation analysis comparing RGS4 and RGS10. Scatter plot of (A) RGS4 and (B) RGS10 3DMTR score (magenta line), permutation analysis score mean (black line), and the standard deviation of the permutation analysis (gray areas).

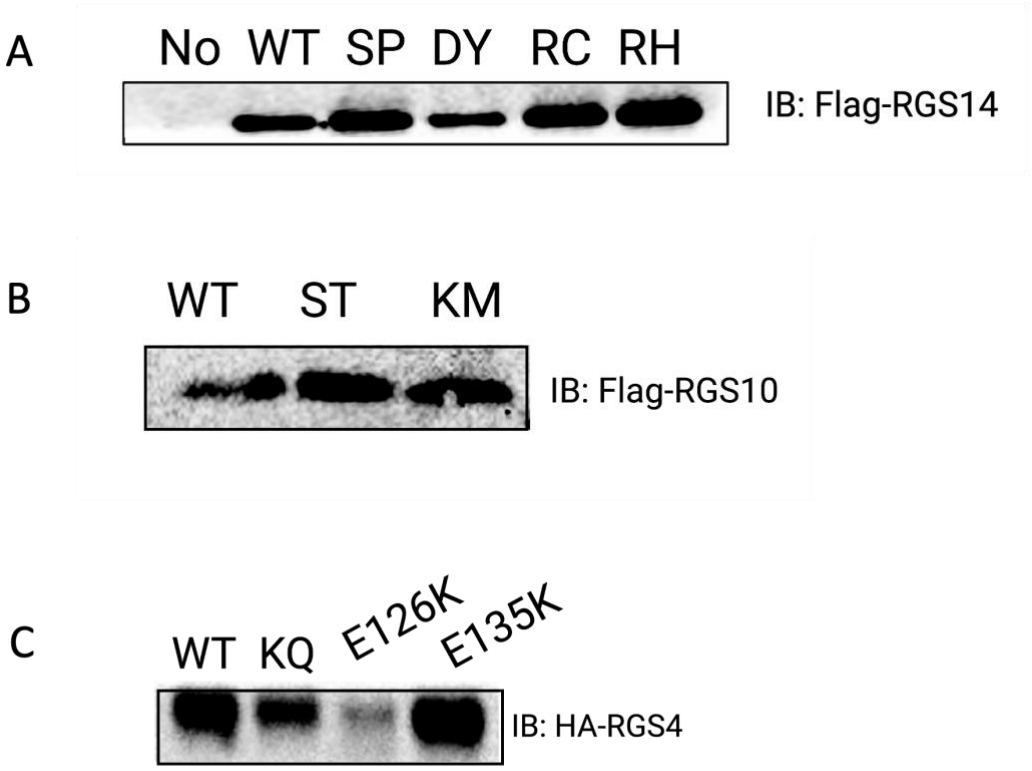

Supplemental Fig 4. RGS WT and mutant protein expression in HEK 293 cells used for Kinetic BRET. To confirm RGS14, RGS10 and RGS4 WT and mutant overexpression, immunoblot analysis was performed. A) Expression of RGS14 and mutants in cells used in Figure 3. B) Expression of RGS10 and mutants in cells used in Figure 4. C) Expression of RGS4 and mutants in cells used in Figure 5.

Supplemental Tables 2-4. Comparison of various bioinformatic tools for their predictive values for change-of-function in amino acids of RGS14, RGS10 and RGS4. Shown are all residues within the RGS domain of RGS14 (S2), RGS10 (S3), and RGS4 (S4) that were identified by 3DMTR analysis to be significant (≤ 0.5) and have reported overlapping cancer mutation. Comparison of the various bioinformatic tools is presented with the score and prediction given to each residue based on the tool's algorithm. Publicly available variant prediction tools used in this analysis were SIFT (Sorting Intolerant From Tolerant; http://sift.jcvi.org), FATHHM (Functional Analysis Through Hidden Markov Models; http://fathmm.biocompute.org.uk), PROVEAN (Protein Variation Effect Analyzer; http://provean.jcvi.org), MutPRED2 (Mutation Predictor; http://mutpred.mutdb.org/).